Collisionless kinetic theory for saltation

Diego Berzi, Alexandre Valance, J.T. Jenkins

Collisionless kinetic theory for saltation

Diego Berzi[1], Alexandre Valance[2] and James T. Jenkins[3]

[1]Department of Civil and Environmental Engineering, Politecnico di Milano, 20133 Milano, Italy

[2]Institut de Physique de Rennes, CNRS UMR 6251, Université de Rennes I, 35042 Rennes, France

[3]School of Civil and Environmental Engineering, Cornell University, Ithaca, NY 14853, USA

We employ the methods of statistical mechanics to obtain closures for the balance equations of momentum and fluctuation kinetic energy that govern the ballistic motion of grains rebounding at a bed driven by turbulent or nonturbulent shearing fluids, in the absence of mid-trajectory collisions. We obtain semi-analytical solutions to steady and fully developed saltation over horizontal, rigid, bumpy beds for the vertical profiles of particle concentration and stresses, and fluid and particle velocity; these compare favorably with measurements in discrete-element numerical simulations in a wide range of conditions that apply to Earth and other planetary environments. The predictions of the particle horizontal mass flux and its scaling with the amount of particles in the system, the properties of the carrier fluid and the intensity of the shearing also agree with numerical simulations and wind tunnel experiments.

I. Introduction

Saltation, that is the motion of solid particles in a gravitational field through successive jumps and rebounds from a base driven by a shearing flow, has been established as the main mode of transport of wind-blown sand (Andreotti 2004; Bagnold 1941; Charru *et al.* 2013; Owen 1964; Valance *et al.* 2015) and is crucial in the dynamics of dunes (Sauermann *et al.* 2001). Although originally conceived as the transport of sand grains by the wind on Earth, it has been recognized as significant also for the transport of sand or gravel in water on Earth (Abbott and Francis 1977; Ancey *et al.* 2002; Fernandez Luque and Van Beek 1976; Niño and García 1998), basalt particles on Venus (Greeley *et al.* 1984; Iversen and White 1982) and on Mars (Iversen *et al.* 1976; Iversen and White 1982), and ice particles on Titan (Burr *et al.* 2015). While these studies considered the carrier fluid to be turbulent, saltation in viscous, non-turbulent fluids has also been investigated (Charru and Mouilleron-Arnould 2002; Ouriemi et al. 2009; Seizilles et al. 2014), given its practical relevance in limiting the transport capacity of oil in pipes (Dall'Acqua *et al.* 2017; Leporini *et al.* 2019).

There is a large body of mathematical models of saltation in the literature (see, e.g., the reviews of Kok et al. 2012; Pähtz et al. 2020; Valance et al. 2015). As highlighted by Valance et al. (2015), the different models can be grouped into two main categories, Lagrangian or Eulerian approaches, based upon the point of view adopted in the description of the particle motion.

In many Lagrangian approaches (Anderson *et al.* 1988; Creyssels *et al.* 2009; Kok and Renno 2009; Werner 1990), an assigned distribution of particle ballistic trajectories is calculated by solving their differential momentum balances, governed by fluid drag and gravity, when immersed in a fluid with a prescribed velocity profile and for a given distribution of initial take-off velocity at the basal boundary. The calculation is repeated once the fluid velocity profile and the distribution of the take-off velocities are updated using a simple constitutive relation for the fluid shear stress (in the case of turbulent fluid, usually based on a mixing length approach) and a suitable set of boundary conditions that govern the impact of the particles at the base (Beladjine *et al.* 2007; Crassous *et al.* 2007; Oger *et al.* 2005), until a steady state is attained.

Simpler Lagrangian approaches in which the distribution of the particle trajectories is replaced by one (Jenkins and Valance 2014) or two (Andreotti 2004) modes have also been recently proposed and

successfully compared against experiments and numerical simulations. In particular, the one species models, also called Periodic Trajectory (PT) models, have been applied to saltation in both turbulent(Berzi *et al.* 2016) and viscous (Valance and Berzi 2022) shearing flows, for values of the ratio of the grain-to-fluid mass densities encountered on Earth and other planetary bodies (Berzi *et al.* 2017). PT models are simple enough to allow even for fully analytical solutions of steady and fully developed saltation, and permit the determination, with sufficient accuracy, of global quantities, such as the particle mass flux, as a function of the intensity of the shearing flows. On the other hand, many variables of interest, such as the distribution with height of the particle concentration and the total depth of the saltation layer, are poorly predicted. It is also not obvious how to extend this model to unsteady and/or boundary-valued (inhomogeneous) problems.

Another family of Lagrangian approaches is based on the framework of Discrete Element Method (DEM, Cundall and Strack 1979), and solves the Newton's laws of motion for the individual grains that are allowed to collide with other particles and with the base, while the surrounding fluid is replaced by discrete forces (such as drag and buoyancy) acting on the particles themselves (Tsuji *et al.* 1993). The forces transmitted by the fluid on the particles are then introduced, after a change of sign, in the fluid momentum balance, ensuring an instantaneous two way coupling. These Discrete-Continuum (DC) numerical simulations are a powerful tool, in that they greatly reduce the number of assumptions necessary to solve for the transport process. For instance, the dynamics of the impact of the particles with the base must not be modelled in advance, but is an output of the simulations. Likewise, the possibility of interparticle collisions above the base is naturally accounted for. On the other hand, the number of particles that is feasible to simulate is severely limited by computational power and nowhere near to the actual number of grains involved in real-scale applications. DC simulations have been applied to saltation in turbulent (Durán *et al.* 2012; Pähtz *et al.* 2015; Pähtz and Durán 2020b; Ralaiarisoa *et al.* 2020) and viscous flows (Valance and Berzi 2022) and provide a large quantity of measurements, some of which are simply unattainable in physical experiments. Hence, they serve as severe tests of more sophisticated approaches.

Eulerian approaches, in which both the fluid and the saltating particles are treated as two superimposed continuum phases offer the most promising perspective for modelling large scale phenomena. In the model of Sauermann et al. (2001), the motion of the two phases is depth-averaged over the saltation layer, and cannot therefore predict the distribution of the variables of interest with height. A key point of the model is that the wind profile in the saltation layer is determined by assuming an exponential distribution of the particle shear stress there. The same assumption is adopted in more recent Eulerian models (Lämmel *et al.* 2012; Pähtz *et al.* 2012). Assuming an *a priori* distribution is crucially different from phrasing a constitutive relation for the particle shear stress, and obtaining the distribution from the usual momentum balance.

Jenkins et al. (2010) were the first to propose a constitutive relation for the particle shear stress based on averaging the equations governing the trajectory of the single particles and substituting averaging of products with products of averaging. They also equated the particle pressure to the product of the particle concentration and the granular temperature, the mean square of the particle velocity fluctuations. They assumed, as in Creyssels et al. (2009), that the latter is uniformly distributed with the distance from the base, which holds only if the vertical drag on the particles is negligible. From the uniform distribution of the granular temperature, they obtained the exponential decay of the particle concentration and distributions of particle and fluid mean horizontal velocities that agreed reasonably well with experiments (Creyssels *et al.* 2009). The model was later extended to deal with unsteadiness and inhomogeneities (Jenkins and Valance 2018). Interestingly, the constitutive relation for the particle shear stress of Jenkins et al. (2010) coincides with the dilute and collisionless limit of the expression derived by Garzó et al. (2012) by solving the Enskog kinetic theory for monodisperse gas-solid flows. This is an indication that both constitutive relations share the same assumption, namely that they only account for the influence of the fluid drag and not gravity nor buoyancy on the particle path.

Here, we formulate a collisionless kinetic theory for saltating particles over an horizontal bed. We distinguish between ascending and descending particles and assume that the velocity distribution function of the ascending particles is an anisotropic Maxwellian, as in Creyssels et al. (2009). Then, we employ approximate analytical expressions for the particle trajectories in viscous and turbulent shearing flows to determine the transfers of horizontal and vertical momentum, and kinetic energy associated with the particle vertical motion across an horizontal surface. Once averaged over all possible particle trajectories using the velocity distribution function, we obtain approximate analytical constitutive relations for the particle stresses and the energy flux of fluctuation kinetic energy.

As suggested by Pasini and Jenkins (2005), collisions above the base can be ignored if the mean free path of kinetic theory is larger than the length of the ballistic trajectory. Given that the mean free path strongly decreases if the particle concentration increases (Chapman and Cowling 1970), and that the particle concentration near erodible beds (composed of particles at rest identical to those in saltation) is large (Tholen *et al.* 2023), we argue that, strictly speaking, collisionless saltation is possible only if it takes place over rigid beds.

We phrase and solve the balances of fluid and particle momenta and particle fluctuation energy for a steady, fully-developed saltation over an horizontal, rigid, bumpy bed, driven by either a viscous or a turbulent shearing flow, in the boundary layer approximation, with appropriate boundary conditions. As in all previous models of saltation, we assume that the fluid velocity is solely in the horizontal direction. This permits to uncouple the determination of quantities associated with the particle vertical motion, such as intensity of the vertical velocity fluctuations, particle concentration and normal stress, from those that involve the particle horizontal motion and are, therefore affected by the flow regime of the fluid, such as particle shear stress and particle and fluid mean horizontal velocity. Depending on the flow regime of the fluid, only one or two differential equations must be solved numerically to determine the vertical profiles of the corresponding quantities. The rest of the profiles, including the depth of the saltation layer, are obtained analytically.

After deriving scaling laws for, e.g., the particle mass flux in some special limits, we successfully test the results of the theory against quasi-2D DC simulations of saltation in viscous and turbulent shearing flows that were carried out suppressing the possibility of mid-trajectory collisions for a wide range of particle-to-fluid mass density ratio, ranging from Mars to Earth environments, at different values of the intensity of the shearing flows, the amount of particles in the system and the viscosity of the fluid. The relation between the particle mass flux and the amount of particles in the system in wind-tunnel experiments (Ho 2012) is also satisfactorily captured.

In Section II, we present the constitutive relations, the balance equations and the boundary conditions that we employ to obtain semi-analytical solutions to steady and fully developed saltation over rigid, bumpy beds. In Section III, we show how to obtain scaling laws for various quantities in the limit of rarefied saltation in both viscous and turbulent flows, at least when the drag coefficient reduces to its asymptotic expressions. Comparisons against DC simulations and experiments are detailed in Section IV. Finally, in Section V, we conclude with a summary of the main findings and an outline of future endeavors.

II. Governing equations and semi-analytical solutions

The saltating particles are identical spheres of diameter d and mass density ρ^s. A shearing flow of a fluid of mass density ρ^f and molecular viscosity μ^f drives the flow in the presence of gravity, with g the gravitational acceleration. The mean horizontal velocities of the particles and the fluid are u and U. We assume that the flow is steady and uniform, so that the velocities are only functions of the vertical distance from the bed y. We imagine that the bed is made bumpy by gluing identical particles of diameter d_w, in close contact to each

other, over a flat plate. Hence, the ratio of d_w to d is a natural measure of the bed roughness. We characterize the particles through the fall particle Reynolds number $\mathrm{R} = \rho^f \sqrt{g\left(r-1\right)/r}d^{3/2} / \mu^f$, where $r = \rho^s/\rho^f$ is the density ratio. A sketch of the flow configuration is shown in Figure 1. In what follows, all quantities are made dimensionless using the diameter and mass density of the particles and the reduced gravitational acceleration, $g(r\text{-}1)/r$. Then, lengths, velocities and stresses are expressed in units of d, $[g(r\text{-}1)d/r]^{1/2}$ and $\rho^s g(r\text{-}1)d/r$, respectively.

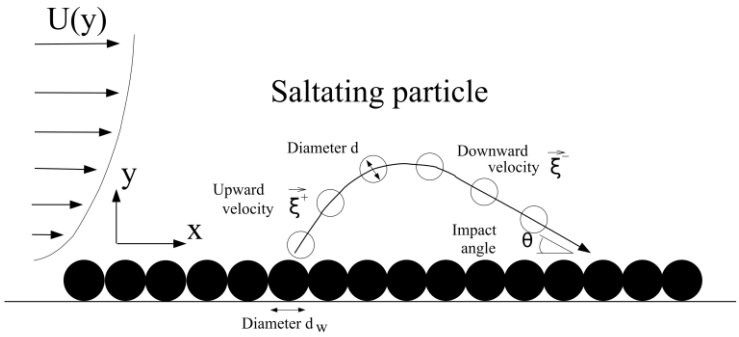

Fig. 1. Sketch of a particle driven into saltation over a rigid, bumpy bed by a shearing flow.

The balance equations for the *x* and *y*-momenta of the particles, under steady and fully-developed conditions, are:

$$\frac{\mathrm{d}\sigma_y}{\mathrm{d}y} = -c; \tag{1}$$

$$\frac{\mathrm{d}s}{\mathrm{d}y} = -cC_D\left(U-u\right), \tag{2}$$

where: σ_y and s are the particle normal stress in the *y*-direction and the particle shear stress, respectively; c is the particle volume concentration; and C_D is the drag coefficient that, for a single particle, has a component independent of the relative velocity between the single particle and the fluid and a component proportional to the absolute value of that velocity difference. Here, we assume that C_D is independent of y and equal to its average over all the spherical particles evaluated at the bed,

$$C_D = \frac{18}{\mathrm{St}} + \frac{0.3}{r}\left|U_0 - u_0\right|, \tag{3}$$

where St = rR is the fall Stokes number, and U_0 and u_0 are the fluid and particle horizontal velocities evaluated at the bed (here and in what follows, the subscript 0 refers to quantities evaluated at the bed). We employ the term *Stokes drag* to refer to situations in which $C_D \simeq 18/\mathrm{St}$, *form drag* for situations in which $C_D \simeq 0.3\left|U_0 - u_0\right|/r$ and *nonlinear drag* for the generic case in which both Stokes and form drag must be accounted for. A more appropriate expression for the average C_D should also involve the strength of the particle velocity fluctuations (Jenkins and Hanes 1998). However, including it would have only a small quantitative effect on the results. Also permitting the drag coefficient to vary along y does not significantly alter the solution to the continuum model.

For flows over rigid beds, we take the no-slip boundary condition for the fluid,

$$U_0 = 0. \tag{4}$$

If saltating particles with a large value of the coefficient of sliding friction impact a rigid bed, made bumpy by gluing identical spheres in close contact on a flat plate, at an average small angle θ with respect to the horizontal (Figure 1), then, using the analysis of Lämmel et al. (2017) in Appendix C,

$$u_0 = \alpha_u \frac{1}{C_D \theta}, \tag{5}$$

where α_u is a strictly positive coefficient of order unity that is weakly dependent on the rebound properties of the particles and the flow regime of the fluid.

In the boundary layer approximation, the sum of the fluid and particle shear stress, *S* and *s* respectively, is constant and equal to the far-field fluid shear stress, which, in dimensionless terms, is the Shields parameter:

$$s + S = \mathrm{Sh}. \tag{6}$$

To close the problem, we require constitutive relations for the particle and fluid stresses.

In the absence of particle collisions above the bed, the only mechanism responsible for the particle stresses is the transfer of momentum associated with the particles crossing a reference surface. Hence, the particle normal stress in the *y*-direction is simply given by the average vertical flux of *y*-momentum,

$$\sigma_y = cT_y, \tag{7}$$

where T_y is the mean square of the vertical velocity fluctuations of the particles.

The distribution of the additional hydrodynamic field, T_y, along *y* is governed by the balance of kinetic energy associated with the particle vertical motion, that is, the *yy*-component of the particle second-moment tensor, which, in a steady and fully-developed flow, and in the absence of mid-trajectory collisions, reduces to (Saha and Alam 2016, 2017)

$$-\frac{\mathrm{d}Q_{yyy}}{\mathrm{d}y} - 2C_D\sigma_y = 0. \tag{8}$$

Here, Q_{yyy} is the *yyy*-element of the flux of second moment, $\mathbf{Q}$, a third rank tensor, and $2C_D\sigma_y$ is the energy dissipation due to the fluid drag.

Assuming that the fluid motion is only horizontal and that the drag coefficient is independent of *y*, we can obtain approximate analytical expressions for the trajectories of the saltating particles even in the turbulent case (Appendix A). In doing so, we distinguish between ascending and descending particles. With the further assumptions that the velocity distribution of the ascending particles is an anisotropic Maxwellian (Creyssels *et al.* 2009) and that the vertical velocity of the ascending particles is much larger than $1/C_D$ (the settling velocity), in Appendix B we derive a simple expression for Q_{yyy}:

$$Q_{yyy} = \sqrt{\frac{8}{\pi}} c^+ \left(T_y^+\right)^{3/2}. \tag{9}$$

where c^+ and T_y^+ are the volume concentration and the mean square of the vertical velocity fluctuations of the ascending particles, respectively. At least under steady state conditions, c^+ and T_y^+ are related to *c* and T_y through (see Appendix B):

$$c = c^+\left(2+\frac{3}{4}C_D\sqrt{\frac{2T_y^+}{\pi}}\right); \tag{10}$$

and

$$T_y = \frac{4\sqrt{\pi}C_D T_y^+ + 4\sqrt{2T_y^+}}{8\sqrt{\pi}C_D + 3{C_D}^2\sqrt{2T_y^+}}. \tag{11}$$

Using equations (7), (10) and (11) into equation (1) leads to

$$\frac{\mathrm{d}c^+}{\mathrm{d}y} = -c^+\frac{8C_D + 3{C_D}^2\sqrt{2T_y^+/\pi}}{4C_D T_y^+ + 4\sqrt{2T_y^+/\pi}} - c^+\frac{2C_D + \sqrt{2/\pi T_y^+}}{2C_D T_y^+ + 2\sqrt{2T_y^+/\pi}}\frac{\mathrm{d}T_y^+}{\mathrm{d}y}, \tag{12}$$

that, combined with equations (8) and (9), permits to obtain an ordinary differential equation for T_y^+:

$$\left[\sqrt{8\pi}C_D\left(T_y^+\right)^{3/2} + 8T_y^+\right]\frac{\mathrm{d}T_y^+}{\mathrm{d}y} = \left(6-4\pi\right){C_D}^2\left(T_y^+\right)^2 - 8T_y^+, \tag{13}$$

whose analytical solution, with the boundary condition $T_y^+\left(y=0\right) = T_{y,0}^+$, is:

$$\begin{aligned}
&4\sqrt{2\pi\left(2\pi-3\right)}\tan^{-1}\left(\frac{C_D}{2}\sqrt{\left(2\pi-3\right)T_y^+}\right)\\
&-2\left(2\pi-3\right)\left[\sqrt{2\pi T_y^+}C_D + 2\log\left(2-iC_D\sqrt{\left(2\pi-3\right)T_y^+}\right) + 2\log\left(2+iC_D\sqrt{\left(2\pi-3\right)T_y^+}\right)\right]\\
&= \left(3-2\pi\right)^2{C_D}^2 y + 4\sqrt{2\pi\left(2\pi-3\right)}\tan^{-1}\left(\frac{C_D}{2}\sqrt{\left(2\pi-3\right)T_{y,0}^+}\right)\\
&-2\left(2\pi-3\right)\left[\sqrt{2\pi T_{y,0}^+}C_D + 2\log\left(2-iC_D\sqrt{\left(2\pi-3\right)T_{y,0}^+}\right) + 2\log\left(2+iC_D\sqrt{\left(2\pi-3\right)T_{y,0}^+}\right)\right].
\end{aligned} \tag{14}$$

Under the same assumptions that we employ to derive equation (5), a simple dependence of $T_{y,0}^+$ calculated at the bed on the impact angle θ can be obtained (Appendix C) in the form:

$$T_{y,0}^+ = \alpha_T\frac{1}{{C_D}^2\theta}\frac{2d_w}{1+d_w}, \tag{15}$$

where α_T is another strictly positive coefficient of order unity that is weakly dependent on the rebound properties of the particles and the flow regime of the fluid. We emphasize that the impact angle, and consequently $T_{y,0}^+$, remains an unknown at this stage of the analysis. We will show how to determine it in the next two sub-sections, when we describe quantities associated with the horizontal motion of the particles, and, therefore, influenced by the flow regime of the fluid.

Equation (14) provides the analytical distribution of T_y^+ along y that, inserted into equation (11), would also give the analytical distribution of T_y. As shown in Figure 2, the latter is roughly linear and well approximated as

$$T_y = \frac{h-y}{h}T_{y,0}, \tag{16}$$

where the depth of the saltation layer, h, is to be determined. The mean square of the particle velocity fluctuations at the bed, $T_{y,0}$, can be obtained from equation (11), if $T_{y,0}^{+}$ is known.

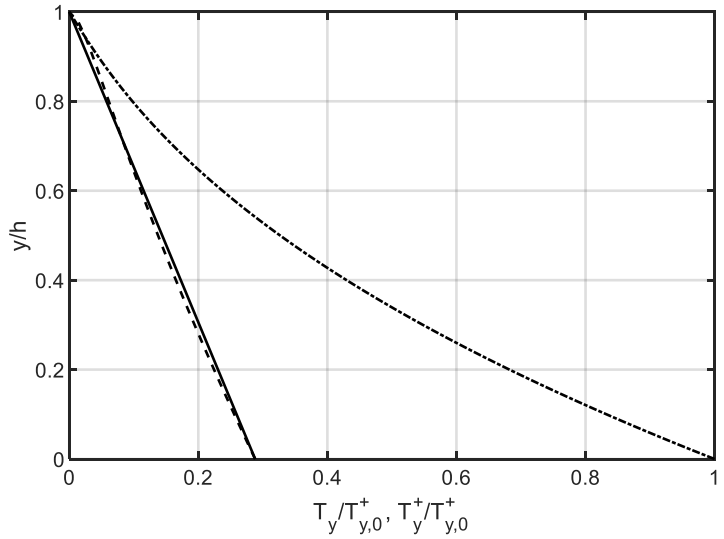

Fig. 2. Normalized profiles of T_y^{+} (dot-dashed line) and T_y (dashed line) obtained from equation (14) and (11), respectively, when C_D = 0.18. The solid line represents the approximate linear distribution of T_y (equation 16).

Inserting equation (7) into equation (1), with equation (16), and integrating gives the following power-law distribution of the particle concentration,

$$c = c_0 \left(\frac{h-y}{h} \right)^{\frac{h-T_{y,0}}{T_{y,0}}}, \tag{17}$$

where c_0 is the particle concentration at the bed. Integrating equation (1) with equation (17) also gives

$$\sigma_y = c_0 T_{y,0} \left(\frac{h-y}{h} \right)^{\frac{h}{T_{y,0}}}. \tag{18}$$

After introducing the particle mass hold-up, $M = \int_0^h c\,dy$, i.e., the particle mass per unit basal area, by integrating equation (1) over the saltation layer, with $\sigma_y = 0$ at $y = h$, we obtain

$$c_0 = \frac{M}{T_{y,0}}. \tag{19}$$

Integrating the energy balance (equation 8) with equations (18) and (19), provides

$$Q_{yyy} = 2C_D M T_{y,0} \frac{h}{h+T_{y,0}} \left[\left(\frac{h-y}{h} \right)^{\frac{h+T_{y,0}}{T_{y,0}}} - 1 \right] + Q_{yyy,0}, \tag{20}$$

where the value of Q_{yyy} at the bed can be obtained from the ratio of equations (9) and (7), with equations (10), (11) and (19), as

$$Q_{yyy,0} = \frac{4C_D T_{y,0}^{+}}{C_D\sqrt{2\pi T_{y,0}^{+}} + 2} M. \tag{21}$$

Given that Q_{yyy} must vanish at the top of the saltation layer, the depth h is determined from equation (20) as

$$h = \frac{Q_{yyy,0}}{2C_D M T_{y,0} - Q_{yyy,0}} T_{y,0}. \tag{22}$$

The governing equations, constitutive relations and analytical results described so far apply, in general, to both saltation in viscous and in turbulent shearing flows and can be calculated only after the determination of the impact angle θ. To proceed, we now must distinguish between the two regimes of the shearing flow.

Before doing that, we support the assumption regarding particle collisions above the bed. As suggested by Pasini and Jenkins (2005), chances of mid-trajectory collisions are low if the mean free path, λ, the average distance travelled by a particle in between two successive collisions predicted by the kinetic theory of granular gases, is less than twice the height of the particle trajectory, here determined by gravity and fluid drag. If we use the expression for the mean free path in a dilute gas of Chapman and Cowling (1970), evaluate this at the bed, and take h as the average height of the particle trajectories, we obtain

$$\lambda_0 = \frac{1}{6c_0\sqrt{2}} \geq 2h. \tag{23}$$

Given that, from equation (22), $h \sim T_{y,0}$, equation (23) implies that there is a maximum mass hold-up M (for given values of r, St and Sh) above which mid-trajectory collisions play a role. The mean free path is a decreasing function of the particle concentration. If the saltation process were to take place over an erodible –a densely packed assembly of particles identical to those in saltation that can be mobilized due to impacts- rather than a rigid bed, and if the volume concentration is continuous across the interface with the erodible bed, then the theoretical mean free path calculated at the top of the erodible bed, where $c \simeq 0.6$, would be much less than the mean free path evaluated at the rigid bed, where $c \ll 1$. Hence, we expect that the mass hold-up at which saltating particles over a rigid bed start to deposit and form an erodible substrate is larger than the maximum mass hold-up for which mid-trajectory collisions can be ignored.

Saltation in viscous shearing flows

In the absence of turbulence, the expression for the fluid shear stress is (Valance and Berzi 2022)

$$S = \frac{1-c}{\mathrm{St}}\frac{\mathrm{d}U}{\mathrm{d}y} \simeq \frac{1}{\mathrm{St}}\frac{\mathrm{d}U}{\mathrm{d}y}, \tag{24}$$

where we have neglected the particle concentration with respect to unity.

Equation (24) implies that, in the absence of particles and in the boundary layer approximation that we have employed, the fluid velocity distribution would be linear. To solve for the particle trajectory, we assume in Appendix A that the fluid velocity profile encountered by an ascending particle during its ballistic trajectory above a certain position y is at least locally linear, in the sense that is linear in the region comprised between y and the top of the trajectory. However, we let the slope of the linear profile to change with y. This assumption and the assumptions that we have already employed in the derivation of the expression for Q_{yyy} in equation (9) permit the derivation in Appendix B of a simple expression for the particle shear stress,

$$s = \frac{3}{5} C_D \sigma_y \left(U - u + \frac{2}{3} \frac{1}{{C_D}^2} \frac{\mathrm{d}U}{\mathrm{d}y} \right). \tag{25}$$

Interestingly, the particle shear stress does not depend on the particle shear rate, as in Jenkins et al. (2010), but only on the velocity difference and on the fluid shear rate. The physical reason is that the particles do not interact with each other, but only with the surrounding fluid.

As explained in Appendix C, the angle θ between the velocity of the particles before the impact with the bed and the horizontal for saltation in viscous flows is estimated as

$$\theta = \frac{C_D}{\mathrm{St}\left(\mathrm{Sh} - s_0\right)}, \tag{26}$$

where s_0 is the particle shear stress at the bed.

Using equations (4) and (5) in equation (3), with equation (26), we obtain a relationship between the drag coefficient and the particle shear stress at the bed,

$${C_D}^3 = \frac{18}{\mathrm{St}} {C_D}^2 + \frac{0.3}{r} \alpha_u \mathrm{St}\left(\mathrm{Sh} - s_0\right). \tag{27}$$

The particle shear stress at the bed is obtained from equation (25), with equations (4), (5), (6), (19) and (24), as

$$s_0 = \frac{\left(2 - 3\alpha_u\right) M \mathrm{StSh}}{5 C_D + \left(2 - 3\alpha_u\right) M \mathrm{St}}, \tag{28}$$

The system of equations (27) and (28) can be solved to determine the drag coefficient and the particle shear stress at the bed once the values of d_w, r, St, Sh and M are given. Then, the impact angle (equation 26), the values of all the variables at the bed (equations 5, 15 and 21), the depth of the saltation layer (equation 22), and the analytical distributions of T_y^+, T_y, c , σ_γ and Q_{yyy} (equations 14, 16-18 and 20) can also be calculated for saltation in viscous shearing flows.

Figure 3 shows the variation of the impact angle, the drag coefficient and the particle shear stress at the bed with the particle mass hold-up, as predicted by equations (26-28), for, e.g., saltation of 100 μm basalt grains in viscous shearing flows on Venus, with α_u = 0.6 (see Section IV for more details about the choice of the parameters). The range of the mass hold-up in Figure 3 is that for which equation (23) is satisfied. Notice that for almost the entire range of mass hold-up, the particle shear stress at the bed linearly increases with M, while θ and C_D are constant.

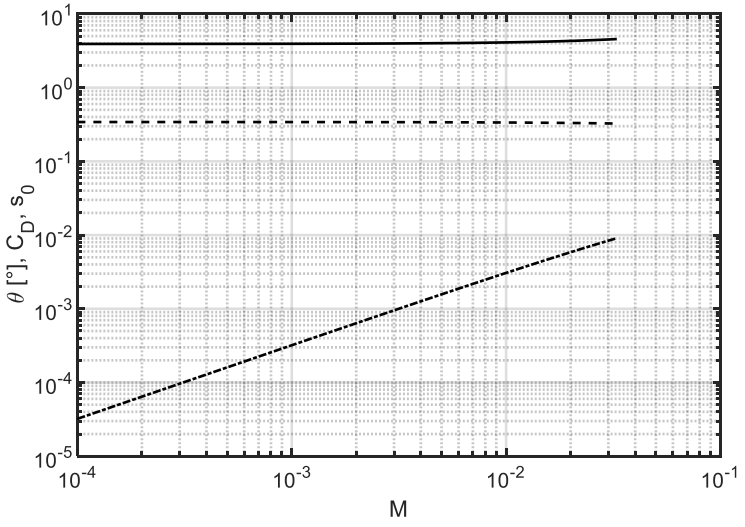

Fig. 3. Predicted impact angle (in degrees, solid line), drag coefficient (dashed line) and particle shear stress at the bed (dot-dashed line) as functions of the mass hold-up for saltation in viscous shearing flows when d_w = 1, St = 100, r = 50, and Sh = 0.05 (with α_u = 0.6).

Using equation (25) in equation (2), with equations (6), (18) and (24), gives a first order, linear, non-homogeneous, differential equation for the particle shear stress,

$$\frac{\mathrm{d}s}{\mathrm{d}y} = -\left[\frac{5}{3}\frac{1}{T_{y,0}}\left(\frac{h-y}{h}\right)^{-1} + \frac{2}{3}\frac{c_0\mathrm{St}}{C_D}\left(\frac{h-y}{h}\right)^{\frac{h-T_{y,0}}{T_{y,0}}}\right]s + \frac{2}{3}\frac{c_0\mathrm{StSh}}{C_D}\left(\frac{h-y}{h}\right)^{\frac{h-T_{y,0}}{T_{y,0}}}. \tag{29}$$

The analytical solution of equation (29) is:

$$\begin{aligned} s = {} & \mathrm{Sh}\left(\frac{2}{3}\frac{M\mathrm{St}}{C_D}\right)^{5/3}\Gamma\left(-\frac{2}{3},\frac{2}{3}\frac{M\mathrm{St}}{C_D}\left(\frac{h-y}{h}\right)^{\frac{h}{T_{y,0}}}\right)\exp\left[\ln\left[\left(\frac{h-y}{h}\right)^{\frac{5}{3}\frac{h}{T_{y,0}}}\right]+\frac{2}{3}\frac{M\mathrm{St}}{C_D}\left(\frac{h-y}{h}\right)^{\frac{h}{T_{y,0}}}\right] \\ & -\mathrm{Sh}\left(\frac{2}{3}\frac{M\mathrm{St}}{C_D}\right)^{5/3}\Gamma\left(-\frac{2}{3},\frac{2}{3}\frac{M\mathrm{St}}{C_D}\right)\exp\left[\ln\left[\left(\frac{h-y}{h}\right)^{\frac{5}{3}\frac{h}{T_{y,0}}}\right]+\frac{2}{3}\frac{M\mathrm{St}}{C_D}\left(\frac{h-y}{h}\right)^{\frac{h}{T_{y,0}}}\right] \\ & +s_0\exp\left[\ln\left[\left(\frac{h-y}{h}\right)^{\frac{5}{3}\frac{h}{T_{y,0}}}\right]+\frac{2}{3}\frac{M\mathrm{St}}{C_D}\left(\frac{h-y}{h}\right)^{\frac{h}{T_{y,0}}}-\frac{2}{3}\frac{M\mathrm{St}}{C_D}\right], \end{aligned} \tag{30}$$

in which Γ is the incomplete gamma function.

The fluid velocity profile is determined by integrating the constitutive relation (equation 24) $\mathrm{d}U/\mathrm{d}y = \mathrm{St}\left(\mathrm{Sh}-s\right)$, with the particle shear stress given by equation (30). Unfortunately, there is no general analytical solution. Hence, we obtain the distribution of U by numerically solving this ordinary differential equation, with the no-slip condition, equation (4), at the bed. Once U is determined, the particle horizontal velocity is given by equation (25) as

$$u = U - \frac{5}{3}\frac{s}{C_D\sigma_y} + \frac{2}{3}\frac{\mathrm{St}\left(\mathrm{Sh}-s\right)}{{C_D}^2}. \tag{31}$$

We can now calculate the particle mass flux q per unit basal area through numerical integration as

$$q = \int_0^h cu\,\mathrm{d}y. \tag{32}$$

In the special case of rarefied saltation, that is for $M \to 0$ and $\mathrm{Sh} \gg s$, the analytical solution of equation (29) simplifies to

$$s = s_0 \left(\frac{h-y}{h} \right)^{\frac{5}{3}\frac{h}{T_{y,0}}} + \frac{M\mathrm{StSh}}{C_D} \left[\left(\frac{h-y}{h} \right)^{\frac{h}{T_{y,0}}} - \left(\frac{h-y}{h} \right)^{\frac{5}{3}\frac{h}{T_{y,0}}} \right], \tag{33}$$

and the fluid velocity profile is simply

$$U = \left(\mathrm{StSh} \right) y. \tag{34}$$

Then, from equations (28), (31), (33) and (34), and the expression for s_0, the particle horizontal velocity is

$$u = \left[\frac{5-2+3\alpha_u}{3} \left(\frac{h-y}{h} \right)^{\frac{2}{3}\frac{h}{T_{y,0}}} + {C_D}^2 y - 1 \right] \frac{\mathrm{StSh}}{{C_D}^2}. \tag{35}$$

Notice that in the rarefied limit of saltation in viscous shearing flows, the particle and the fluid velocity profiles are independent of the mass hold-up. Using equations (17), (19) and (35) in equation (32), and integrating, gives

$$q = M\mathrm{StSh}T_{y,0} \frac{h}{h+T_{y,0}}. \tag{36}$$

Saltation in turbulent shearing flows

In the case of saltation in turbulent shearing flows, we model the fluid shear stress using the classical mixing length approach (Jenkins *et al.* 2010),

$$S = \frac{1-c}{r} \kappa^2 \left(y + y_0 \right)^2 \left(\frac{dU}{dy} \right)^2 \simeq \frac{\kappa^2 \left(y + y_0 \right)^2}{r} \left(\frac{dU}{dy} \right)^2, \tag{37}$$

where $\kappa = 0.41$ is Von Kármán's constant and $y_0 = \frac{1}{9\mathrm{St}} \sqrt{\frac{r}{\mathrm{Sh}}} + \frac{k_s}{30} \left[1 - \exp\left(-k_s \frac{\mathrm{St}}{26} \sqrt{\frac{\mathrm{Sh}}{r}} \right) \right]$ is an expression for the origin of the logarithmic fluid velocity profile that encompasses hydrodynamically smooth, rough and transitional beds (Guo and Julien 2007). The roughness length scale k_s is taken to be $k_s = d_w$ (Ho 2012).

Equation (37) implies that, in the absence of particles and in the boundary layer approximation that we have employed, the fluid velocity distribution would be logarithmic. We assume that the fluid velocity profile encountered by an ascending particle during its ballistic trajectory above a certain position y is uniform and equal to the average of the logarithmic profile in the region comprised between y and the top of the trajectory. This average value of U changes with y. This assumption, and the assumptions that we have already employed in the derivation of the expression for Q_{yyy}, equation (9), permits the derivation in Appendix B of an expression for the particle shear stress,

$$s=\frac{3}{5}C_D\sigma_y\left[U-u+\frac{3}{4}\frac{\sqrt{rS}}{\kappa}\ln\left(\frac{\kappa}{C_D}\sqrt{\frac{T_y^+}{rS}}\frac{dU}{dy}+1\right)\right]. \tag{38}$$

As in the viscous case of equation (25), the particle shear stress in turbulent shearing flows does not depend on the particle shear rate. The saltating particles, when treated as a continuous medium, can experience shear stress even if the horizontal particle velocity is uniform in the flow domain.

As explained in Appendix C, the impact angle θ for saltation in turbulent flows is estimated as

$$\theta\simeq\left[0.85C_D\frac{\sqrt{r\left(\mathrm{Sh}-s_0\right)}}{\kappa}\ln\left(\frac{1}{C_D}\frac{\sqrt{T_{y,0}^+}}{y_0}\right)\right]^{-1}. \tag{39}$$

Using equation (5) in equation (3) gives the drag coefficient in terms of the impact angle,

$$C_D=\frac{9}{\mathrm{St}}+\frac{1}{2}\sqrt{\left(\frac{18}{\mathrm{St}}\right)^2+\frac{1.2}{r}\alpha_u\frac{1}{\theta}}. \tag{40}$$

Equation (38) evaluated at the bed, with equations (5) and (39) also gives the particle shear stress at the bed as a function of the impact angle,

$$s_0=\frac{3}{5}\frac{M}{\theta}\left(0.9-\alpha_u\right), \tag{41}$$

Then, equation (39) with equations (15), (40) and (41) results in a transcendental equation for θ,

$$\begin{aligned}\frac{1}{\theta}\left(\frac{9}{\mathrm{St}}+\frac{1}{2}\sqrt{\left(\frac{18}{\mathrm{St}}\right)^2+\frac{1.2}{r}\alpha_u\frac{1}{\theta}}\right)^{-1}&\simeq\frac{0.85}{\kappa}\sqrt{r\left(\mathrm{Sh}-\frac{3}{5}M\left(0.9-\alpha_u\right)\frac{1}{\theta}\right)}\\&\times\ln\left[\frac{1}{y_0}\left(\frac{9}{\mathrm{St}}+\frac{1}{2}\sqrt{\left(\frac{18}{\mathrm{St}}\right)^2+\frac{1.2}{r}\alpha_u\frac{1}{\theta}}\right)^{-2}\sqrt{\frac{\alpha_T}{\theta}\frac{2d_w}{1+d_w}}\right],\end{aligned} \tag{42}$$

that can be solved to determine the impact angle. Once θ is known, C_D (equation 40), s_0 (equation 41), the boundary values of the remaining variables at the bed (equations 5, 15 and 21), the depth of the saltation layer (equation 22), and the analytical distributions of T_y^+, T_y, c , σ_y and Q_{yyy} (equations 14, 16-18 and 20) can also be calculated for saltation in turbulent shearing flows.

Figure 4 shows the variation of the impact angle, the drag coefficient and the particle shear stress at the bed with the particle mass hold-up, as predicted by equations (40-42), for, e.g., saltation of 240 μm sand grains in a turbulent wind on Earth, with α_u = 0.8 and α_T = 1 (see Section IV for more details about the choice of the parameters). The range of the mass hold-up in Figure 4 is that for which equation (23) is satisfied. As for saltation in viscous shearing flows (Figure 3), the particle shear stress at the bed linearly increases with M, while θ and C_D are almost constant.

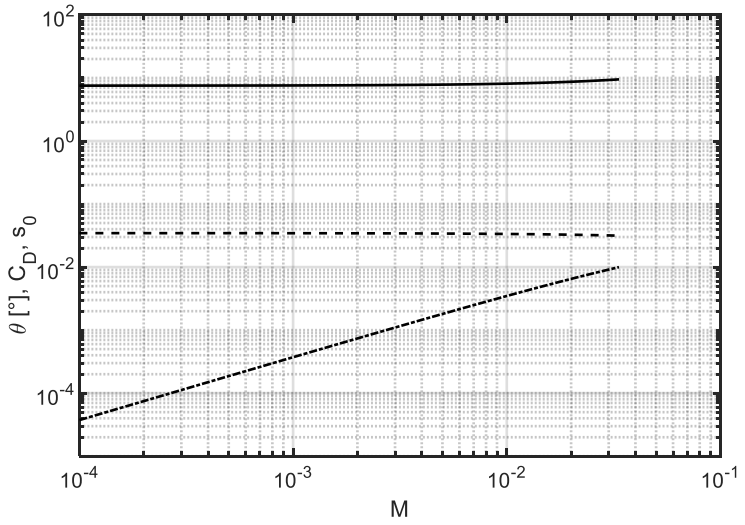

Fig. 4. Predicted impact angle (in degrees, solid line), drag coefficient (dashed line) and particle shear stress at the bed (dot-dashed line) as functions of the mass hold-up for saltation in turbulent shearing flows with d_w = 1.5, St = 1681, r = 2208, and Sh = 0.04 (with α_u = 0.8 and α_T= 1).

Equation (2), with equations (38) and (6), and equation (37) can be written as a system of two ordinary differential equations:

$$\frac{\mathrm{d}s}{\mathrm{d}y} = \frac{3}{4} C_D c \frac{\sqrt{r\left(\mathrm{Sh} - s\right)}}{\kappa} \ln\left(\frac{1}{C_D} \frac{\sqrt{T_y^+}}{y + y_0} + 1 \right) - \frac{5}{3} \frac{s}{T_y}; \tag{43}$$

,

and

$$\frac{\mathrm{d}U}{\mathrm{d}y} = \frac{\sqrt{r\left(\mathrm{Sh} - s\right)}}{\kappa\left(y + y_0\right)}; \tag{44}$$

these can be numerically integrated, with the boundary conditions of equations (4) and (41), to obtain the distributions of the particle shear stress and the fluid horizontal velocity. Then, the particle horizontal velocity is given by equation (38), with equation (6), as

$$u = U + \frac{3}{4} \frac{\sqrt{r\left(\mathrm{Sh} - s\right)}}{\kappa} \ln\left(\frac{1}{C_D} \frac{\sqrt{T_y^+}}{y + y_0} + 1 \right) - \frac{5}{3} \frac{s}{C_D \sigma_y}. \tag{45}$$

Finally, the particle mass flux q per unit basal area is determined through numerical integration of equation (32), with the profiles of u and c obtained under turbulent conditions.

III. Scaling laws for rarefied saltation

The semi-analytical solutions to particle saltation in shearing flows described in the previous section permit simple scalings to be obtained, at least in the extreme cases of rarefied saltation, that is for $M \to 0$ and $s_0 \ll \mathrm{Sh}$, when there is only Stokes drag – $C_D = 18/\mathrm{St}$, when the particle Reynolds number based upon the relative velocity between the particles and the fluid at the bed, $u_0 \mathrm{St}/r$, is less than unity, or form drag –

$C_D = 0.3u_0/r$, when $10^3 < u_0\mathrm{St}/r < 10^5$. In the following, we will consider that at leading order, equations (11) and (22) imply that $T_{y,0} \propto h \propto {T_{y,0}}^{+1/2}/C_D$.

We emphasize that there is no feedback of the particles on the fluid velocity profile, which, in rarefied saltation, is exactly linear in the viscous case, and logarithmic in the turbulent case. As a consequence, the particle mass hold-up only affects the particle concentration, and it is linearly proportional to it, and does not influence the particle velocity. Given that the mass flux involves the product of particle concentration and horizontal velocity, *q* must also be linearly related to the mass hold-up.

Rarefied saltation in viscous shearing flows with Stokes drag

In this case, the density ratio plays no role in the equations governing the saltation process. As mentioned, $C_D \propto \mathrm{St}^{-1}$. Then, with equation (26), we obtain that $\theta \propto \mathrm{St}^{-2}\mathrm{Sh}^{-1}$. With this, equations (5), (15), (19) and (36) imply the scalings for the various quantities that we report in Table 1. In particular, we notice that the scaling for the mass flux, $q \propto M\mathrm{St}^4\mathrm{Sh}^{3/2}$, was also derived in Valance and Berzi (2022) by using an approach in which all particles were assumed to follow the same periodic trajectory, and not a distribution of trajectories as in the present work.

Rarefied saltation in viscous shearing flows with form drag

In the case of form drag, $C_D \propto u_0 r^{-1}$. Then, we expect the scaling laws to involve also the density ratio. With equation (5), we obtain $u_0 \propto r^{1/2}\theta^{-1/2}$, and, with equations (26) and (15), $\theta \propto r^{-1/3}\mathrm{St}^{-2/3}\mathrm{Sh}^{-2/3}$ and ${T_{y,0}}^+ \propto r$. Hence, equations (5), (15), (19) and (36) imply the scalings for the various quantities that we report in Table 1.

Rarefied saltation in turbulent shearing flows with form drag

In this limiting case, the fall Stokes number, St, plays no role in the equations governing the saltation process and cannot be involved in the scalings. With $C_D \propto u_0 r^{-1}$ and equation (5), we obtain $u_0 \propto r^{1/2}\theta^{-1/2}$, and, with equations (41) and (15), at leading order, $\theta \propto \mathrm{Sh}^{-1}$ and ${T_{y,0}}^+ \propto r$. Hence, $u_0 \propto r^{1/2}\mathrm{Sh}^{1/2}$, $C_D \propto r^{-1/2}\mathrm{Sh}^{1/2}$, and $h \propto T_{y,0} \propto {T_{y,0}}^{+1/2}/C_D \propto r\mathrm{Sh}^{-1/2}$. Equation (19), then, provides $c_0 \propto Mr^{-1}\mathrm{Sh}^{1/2}$. As shown later, the concentration and particle velocity profiles in the case of turbulent saltation are approximately uniform along *y*. Therefore, we expect $q \propto c_0 u_0 h \propto M\mathrm{Sh}^{1/2}r^{1/2}$. We summarize the scaling laws for rarefied turbulent saltation with form drag in Table 1.

Table 1. Summary of the scaling laws for rarefied saltation.

	Viscous saltation with Stokes drag	Viscous saltation with form drag	Turbulent saltation with form drag
Drag coefficient, C_D	St^{-1}	$\mathrm{St}^{1/3}\mathrm{Sh}^{1/3}r^{-1/3}$	$\mathrm{Sh}^{1/2}r^{-1/2}$
Impact angle, θ	$\mathrm{St}^{-2}\mathrm{Sh}^{-1}$	$\mathrm{St}^{-2/3}\mathrm{Sh}^{-2/3}r^{-1/3}$	Sh^{-1}
Particle slip velocity, u_0	$\mathrm{St}^3\mathrm{Sh}$	$\mathrm{St}^{1/3}\mathrm{Sh}^{1/3}r^{2/3}$	$\mathrm{Sh}^{1/2}r^{1/2}$
Depth of saltation layer, h	$\mathrm{St}^3\mathrm{Sh}^{1/2}$	$\mathrm{St}^{-1/3}\mathrm{Sh}^{-1/3}r^{5/6}$	$r\mathrm{Sh}^{-1/2}$
Particle concentration at the bed, c_0	$M\mathrm{St}^{-3}\mathrm{Sh}^{-1/2}$	$M\mathrm{St}^{1/3}\mathrm{Sh}^{1/3}r^{-5/6}$	$M\mathrm{Sh}^{1/2}r^{-1}$
Particle mass flux, q	$M\mathrm{St}^4\mathrm{Sh}^{3/2}$	$M\mathrm{St}^{2/3}\mathrm{Sh}^{2/3}r^{5/6}$	$M\mathrm{Sh}^{1/2}r^{1/2}$

IV. Comparisons with numerical simulations and experiments

Here, we make comparisons between the predictions of the present theory and the results of discrete-continuum numerical simulations of saltation of spheres over a rigid bumpy bed made of a layer of particles identical to those saltating in close contact. The simulations are performed in a quasi-2D cell of streamwise length equal to 5120 particle diameters and transverse width equal to one particle diameter, with periodic boundary conditions in the streamwise direction. The cell is not upper-bounded.

We solve Newton's equations of motion for the individual spherical particles under the influence of fluid drag, buoyancy, gravity and contact forces when they collide with the bed (mid-trajectory collisions are forbidden), while treating the fluid as either a viscous or a turbulent continuum, depending on the closure for the fluid shear stress, for which balance equations are phrased. Once changed in sign, the sum over all particles of drag and buoyancy enter the momentum balance for the fluid, thus ensuring the two-way coupling between the phases. In the numerical simulations, we assume that the fluid only possesses horizontal velocity and we suppress the possibility of interparticle collisions above the bed. The individual particles experience a fluid drag based upon the local difference between the instantaneous velocity of the particle and the average velocity of the fluid. As in our theoretical treatment, we control the amount of particles in the simulations –the particle mass hold-up, M, the bumpiness of the rigid bed –the wall-particle diameter, d_w, the viscosity –the inverse of the fall Stokes number, St, the mass density –the inverse of the density ratio, r, of the fluid, and the intensity of the shearing flow –the Shields number, Sh. In what follows, all measurements have been taken once a steady state is attained and, subsequently, time-averaged. This type of numerical simulations have already been used in the context of saltation in both turbulent (Durán *et al.* 2012; Pähtz *et al.* 2015; Pähtz and Durán 2020a; Ralaiarisoa *et al.* 2020) and viscous (Valance and Berzi 2022) shearing flows. A more detailed description of the numerical simulations, including the contact parameters that we employ, can be found in Appendix D.

In a total of 50 simulations, we have numerically investigated the saltation process of four different types of solid particles in terrestrial and extra-terrestrial environment, as summarized in Table 2, by changing the mass hold-up between 0.0004 and about 0.03 that is from the rarefied limit to the maximum mass hold-up for which the mid-trajectory collisions can be neglected and equation (23) is satisfied. Although the fluid regime on Mars and Venus is almost certainly turbulent, one can at least imagine performing experiments in pressurized wind-tunnels, in which the turbulence is somehow suppressed, thus recovering the conditions reported in the first two rows of Table 2. The conditions reported in the last two rows of Table 2 are, instead, much closer to actual physical applications.

The chosen flow conditions serve the purpose of isolating and testing the assumptions that we have made in building our theory: (i) anisotropic Maxwellian velocity distribution for the particles, vertical velocity of the ascending particles much larger than the settling velocity and locally linear velocity for the fluid in the case of viscous regime and Stokes drag –first row in Table 2; (ii) additional assumption of drag coefficient uniform and equal to that evaluated at the bed in the case of viscous regime and nonlinear drag –second and third row in Table 2; and (iii) fluid velocity profile encountered by an ascending particle uniform and equal to the average of the logarithmic profile in the case of turbulent regime and nonlinear drag –fourth row in Table 2.

The parameters of the turbulent case in Table 2 match those of physical experiments of saltation on rigid, bumpy beds performed in a wind-tunnel (Ho 2012); for these, measurements of particle mass flux and profiles of particle concentration and horizontal particle and fluid velocities at different values of the particle mass hold-up are available. In the experiments, unlike the numerical simulations, the vertical velocity of the fluid surrounding the particles is nonzero, due to the no-slip condition on the particle surface, and this would permit a test of its influence on the results. However, as shown later, the depth of the saltation layer in the

absence of an upper bound predicted by our model and measured in the numerical simulations is of the order of 4000 particle diameters. The experiments were performed in a rectangular closed conduit, with an horizontal lid placed at about 1200 particle diameters above the rigid base. As a consequence, the top boundary conditions are different from those of the present numerical simulations and the semi-analytical treatment. Although the order of magnitude of the profiles measured in the experiments is in good agreement with our model, their shape reveals the influence of the upper boundary. We postpone to a future work the solution of the appropriate two-point boundary value problem, with our proposed constitutive relations for the particle stresses and energy flux, and detailed comparisons against the experimental measurements.

Table 2. Summary of the combination of parameters employed in the numerical simulations.

Description	Regime	St	r	Sh	d_w
60 or 75 μm basalt particles on Mars	viscous (Stokes drag)	60, 100	150000	0.05, 0.075	1
100 μm basalt particles on Venus	viscous (nonlinear drag)	100	50	0.05	1
650 μm sand particles in water on Earth or,equivalently, 3 mm sand particles in crude oil on Earth	viscous (nonlinear drag)	100	2.5	0.05	1
240 μm sand particles in air on Earth	turbulent (nonlinear drag)	1681	2208	0.025, 0.04	1.5

Figures 5 and 6 show the comparisons between profiles of T_y, c, σ_y, s, u and U relative to selected values of the mass hold-up (similar agreement, not shown here for brevity, is obtained for all admissible values of M) for saltation in viscous shearing flows with Stokes drag –first column of plots in both figures, saltation in viscous shearing flows with nonlinear drag –second column, and saltation in turbulent shearing flows with nonlinear drag –third column. In determining the semi-analytical solution that we have highlighted in Section II, we have employed $\alpha_u = 0.6$ and $\alpha_T = 0.5$ for saltation in viscous flows, and $\alpha_u = 0.8$ and $\alpha_T = 1$ for saltation in turbulent flows. Different values of these parameters would not alter the qualitative features of our semi-analytical solution, but only slightly impact the values of T_y, c and u at the bed, therefore causing a shift to the right or to the left in the relative profiles.

Figures 5(a-c) confirm that the intensity of the velocity fluctuations of the particles decreases linearly with the distance from the rigid bed, and the model captures both the weak dependence of T_y on M for viscous saltation and Stokes drag (Figure 5a), and its independence for nonlinear drag (Figures 5b and c). The depth of the saltation layer is well predicted by the continuum model, but the slope of the linear decrease is underestimated with respect to the numerical simulations for nonlinear drag. Also, the nonmonotonic behaviour of T_y near the rigid bed is not captured. These are the consequences of neglecting the dependence of the drag coefficient on the vertical direction. The agreement with the measurements in the numerical simulations would indeed improve if C_D is allowed to vary locally; however, this prevents our obtaining semi-analytical solutions of the governing equations, with little gain on the results.

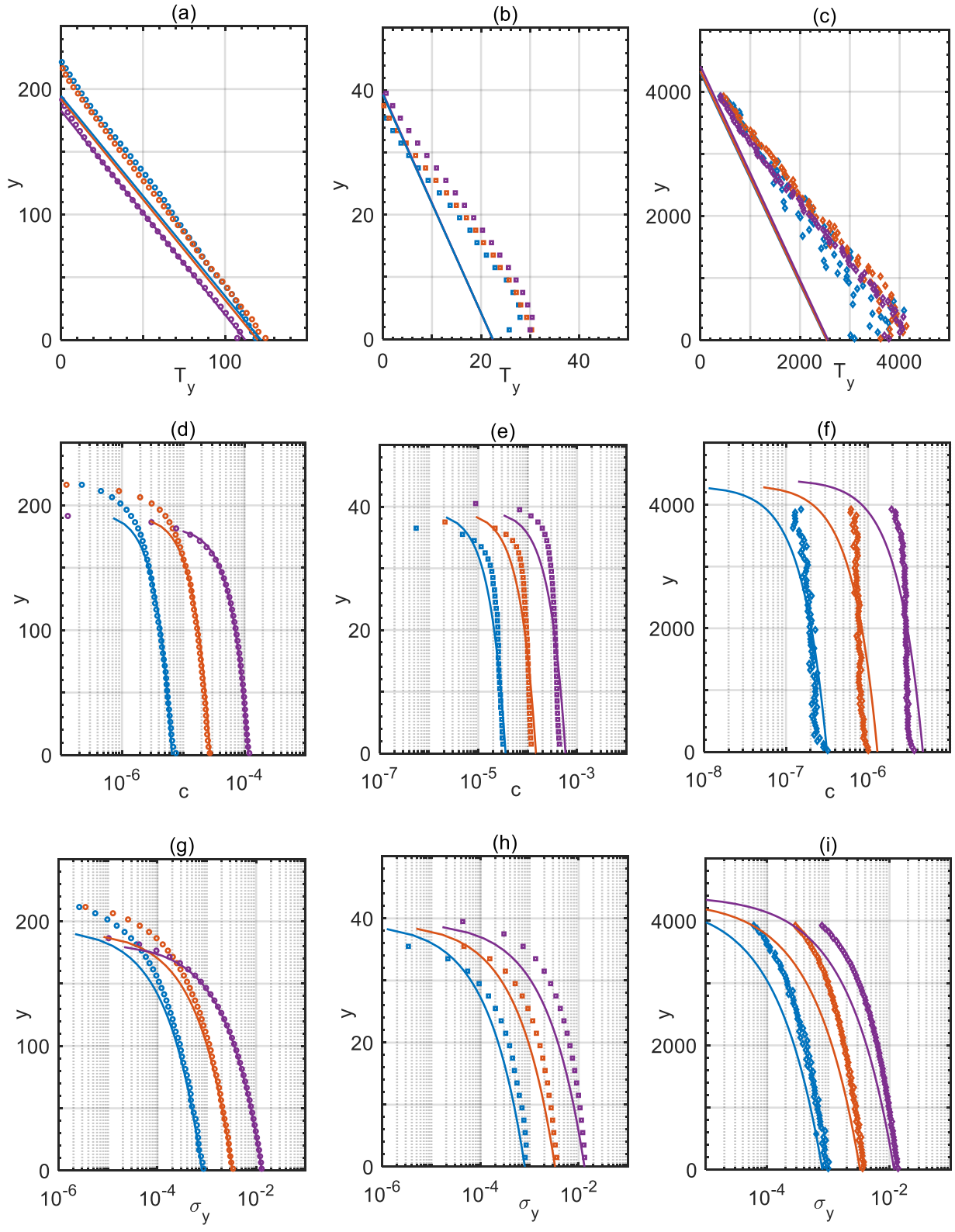

Fig. 5. Profiles of (a-c) mean square of particle velocity fluctuations in the vertical direction, (d-f) particle concentration and (g-i) particle normal stress along y measured in numerical simulations of: saltation in viscous shearing flows with d_w = 1, St = 100, r = 150000, Sh = 0.05 and M = 0.0008 (blue circles), M = 0.0033 (red circles), M = 0.0131 (purple circles); saltation in viscous shearing flows with d_w = 1, St = 100, r = 50, Sh = 0.05 and M = 0.0008 (blue squares), M = 0.0033 (squares), M = 0.0131 (purple squares); saltation in turbulent shearing flows with d_w = 1.5, St = 1681, r = 2208, Sh = 0.04 and M = 0.0008 (blue diamonds), M = 0.0033 (red diamonds), M = 0.0119 (purple diamonds). The solid lines are the predictions of the present theory.

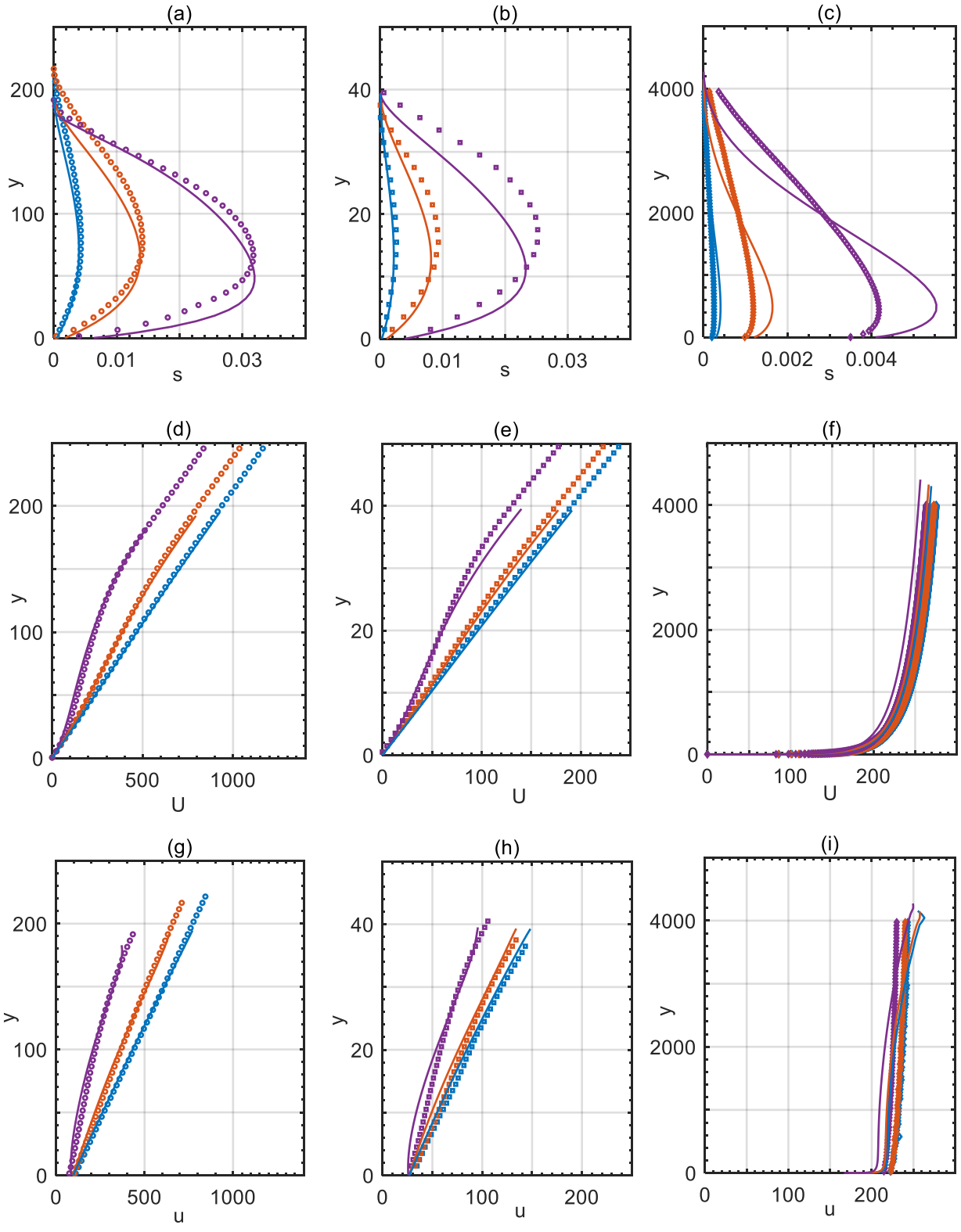

Fig. 6. Profiles of (a-c) particle shear stress, (d-f) fluid and (g-i) particle mean horizontal velocities measured in numerical simulations of: saltation in viscous shearing flows with $d_w = 1$, St = 100, $r = 150000$, Sh = 0.05 and $M = 0.0008$ (blue circles), $M = 0.0033$ (red circles), $M = 0.0131$ (purple circles); saltation in viscous shearing flows with $d_w = 1$, St = 100, $r = 50$, Sh = 0.05 and $M = 0.0008$ (blue squares), $M = 0.0033$ (squares), $M = 0.0131$ (purple squares); saltation in turbulent shearing flows with $d_w = 1.5$, St = 1681, $r = 2208$, Sh = 0.04 and $M = 0.0008$ (blue diamonds), $M = 0.0033$ (red diamonds), $M = 0.0119$ (purple diamonds). The solid lines are the predictions of the present theory.

In all cases, the continuum model satisfactorily reproduces the profiles of particle concentration and normal stress in the *y*-direction (Figures 5d-i), which indeed follow the power-law distributions of equations (17) and (18). In the turbulent case, as anticipated, the particle concentration is rather uniform along *y* (Figure 5f). The values of the particle concentration are also much smaller in the case of turbulent shearing flows (Figure 5f), as a consequence of the greater agitation of the particles (Figure 5c).

Figure 5 shows only profiles of quantities associated with the vertical motion of the saltating particles, which is entirely uncoupled from the horizontal motion of the fluid in our continuum model and in the numerical simulations, were it not for the dependence of the drag coefficient on *U*. The horizontal motion of the fluid, and in particular its flow regime, strongly affects the distribution of particle shear stress and particle and fluid horizontal velocity shown in Figure 6.

Our proposed constitutive relations for the particle shear stress (equations 25 and 38) permit the qualitatively and quantitatively reproduction of the measurements in numerical simulations (Figures 6a-c). In particular, the position and the magnitude of the peak in the particle shear stress are well captured. The physical reason for the presence of this maximum value of the particle shear stress above the bed is in the change of sign of the horizontal force exerted by the fluid on the particles. The particles slip at the rigid bed, while the fluid does not; hence, the particles drag the fluid near the bed, while the fluid drags the particles as the top of the saltation layer is approached. Interestingly, the particle shear stress can reach values up to 50-60 % of the total shear stress –the Shields parameter– for saltation in viscous shearing flows, but only up to 10 % of the total shear stress for saltation in turbulent shearing flows.

As the mass hold-up increases, the fluid and particle horizontal velocity profiles become progressively nonlinear for saltation in viscous shearing flows (Figures 6d, e, g and h), but the continuum model is capable of capturing this behaviour. For saltation in turbulent shearing flows, the fluid velocity profile is logarithmic, and the mass hold-up has little influence on it (Figure 6f). The horizontal velocity of the particles is almost uniform vertically (Figure 6i). This confirms our finding that in the absence of particle interactions, the particle shear stress does not depend on the particle shear rate. The slight discrepancies between the predictions of the continuum model and the results of the numerical simulations are a seemingly minor consequence of the lack of perfect agreement in terms of particle shear stress (Figure 6c).

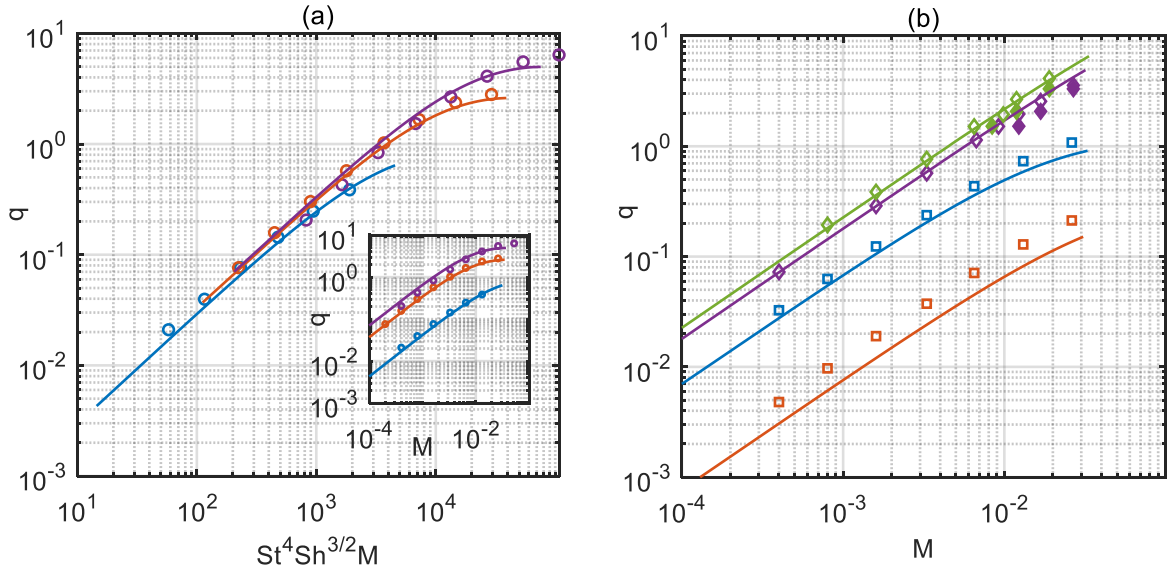

Fig. 7. (a) Particle mass flux against scaled particle mass hold-up measured in discrete-continuum numerical simulations (open symbols) and predicted from the present theory (lines) in the case of saltation in viscous shearing flows with $d_w = 1$, $r = 150000$ and: St = 60 and Sh = 0.05 (blue circles); St = 100 and Sh = 0.05 (orange circles); St = 100 and

Sh = 0.075 (purple circles). The inset depicts the same data in terms of q against M. (b) Particle mass flux against particle mass hold-up measured in discrete-continuum numerical simulations (open symbols) and in wind-tunnel experiments (filled symbols, after Ho 2012) and predicted from the present theory (lines) in the case of saltation in viscous shearing flows with d_w = 1.5, St = 100 Sh = 0.05, and r = 2.5 (orange squares) and r = 50 (blue squares); and in the case of saltation in turbulent shearing flows with d_w = 1.5, St = 1681, r = 2208, and Sh = 0.025 (purple diamonds) and Sh = 0.04 (green diamonds).

Finally, we compare the dependence of the particle mass flux on the particle mass hold-up in Figure 7. The continuum model notably reproduces the measurements in numerical simulations in both the viscous and turbulent shearing flows. The experimental results on turbulent saltation in a wind-tunnel (Ho 2012) are in sufficiently good agreement with both the numerical simulations and the continuum model (Figure 7b). The overestimate of the experimental mass flux is likely due to the additional resistance induced by the presence of the horizontal lid above the rigid bed, that we do not account for. Figure 7a also assesses the validity of the scaling for q reported in Table 1 for the case of viscous saltation and Stokes drag, in the rarefied limit.

V. Conclusions

We have derived constitutive relations for the particle stresses and flux of particle kinetic energy associated with the fluctuating vertical velocities that apply to saltation of particles in viscous and turbulent shearing flows, in the absence of collisions above the bed. To do this, we have employed the averaging methods of statistical mechanics based on an anisotropic Maxwellian velocity distribution function for the ascending particles and approximate analytical expressions for the particle trajectories under the influence of fluid drag, gravity and buoyancy.

Given that we neglect the possibility of particle-particle interactions, we have obtained the perhaps unexpected result that the particle shear stress does depend on the local relative velocity between the grains and the carried fluid and the fluid shear rate, but not on the particle shear rate. We have combined the constitutive relations for the particle phase and well-known expressions for the fluid shear stress with momentum and energy balances to obtain semi-analytical solutions of steady, fully-developed saltation over horizontal, rigid beds. We have employed boundary conditions appropriated for particles rebounding at a bumpy base with no upper-bounds, and assumed that the carrier fluid has only mean horizontal velocity. Hence, the regime of the carrier fluid, viscous or turbulent, does not affect the profiles of particle concentration and normal stress, which follow a power-law decrease with height, and mean square of the vertical velocity fluctuations, linearly decreasing with the distance from the bed. These results are in contrast with previous theoretical and experimental works in which the granular temperature was assumed to be uniform and the concentration was shown to decrease exponentially with height.

We have confirmed our findings through extensive comparisons with discrete-continuum simulations in both viscous and turbulent regime. Thus, we are inclined to blame mid-fluid collisions for the above mentioned qualitative difference in the distribution of particle concentration. We have also shown that the predictions of the theory in terms of profiles of particle shear stress, and particle and fluid mean horizontal velocity are in excellent agreement with the numerical simulations. In natural units of particle mass density, diameter and reduced gravity, we have determined that the saltation process is controlled by the mass of particles in the system, the intensity of the shearing flow, the fluid mass density and viscosity and the bumpiness of the rigid base.

We have successfully tested the dependence of the horizontal mass flux per unit basal area of the particles as a function of the mass hold-up obtained with our theory against discrete-continuum numerical simulations and wind-tunnel experiments, for a large range of the control parameters. We have also

determined simple scaling laws for the dependence of various quantities of interest on the control variables in the special limits of rarefied viscous and turbulent saltation, and solely Stokes or form drag on the particles.

In a future, we plan to apply our theory to two-point boundary value problems, to, e.g., mimic available experiments of saltation in enclosed wind-tunnels. We also wish to extend the present work to deal with unsteady and /or developing flows. More importantly, the inclusion of mid-fluid collisions, that is the transition from a collisionless to a collisional kinetic theory of saltation, is a crucial future step, especially in view of modelling transport phenomena over erodible beds, of more interest for geophysical and planetary science applications.

Declaration of interests. The authors report no conflict of interest.

References

Abbott, JE, and Francis, JRD (1977) Saltation and Suspension Trajectories of Solid Grains in a Water Stream. *Philosophical Transactions of the Royal Society A: Mathematical, Physical and Engineering Sciences*, **284**(1321), 225–254. doi:10.1098/rsta.1977.0009.

Ancey, C, Bigillon, F, Frey, P, Lanier, J, and Ducret, R (2002) Saltating motion of a bead in a rapid water stream. *Physical Review E*, **66**(3), 036306. doi:10.1103/PhysRevE.66.036306.

Anderson, RS, Haff, PK, Anderson, RS, and Haff, PK (1988) Simulation of Eolian Saltation. *Science*, **241**(4867), 820–823.

Andreotti, B (2004) A two-species model of aeolian sand transport. *Journal of Fluid Mechanics*, **510**, 47–70. doi:10.1017/S0022112004009073.

Bagnold, RA (1941) *The Physics of Blown Sand and Desert Dunes*, New York: Methuen.

Beladjine, D, Ammi, M, Oger, L, and Valance, A (2007) Collision process between an incident bead and a three-dimensional granular packing. *Physical Review E*, **75**(6), 061305. doi:10.1103/PhysRevE.75.061305.

Berzi, D, Jenkins, JT, and Valance, A (2016) Periodic saltation over hydrodynamically rough beds: aeolian to aquatic. *Journal of Fluid Mechanics*, **786**, 190–209. doi:10.1017/jfm.2015.601.

Berzi, D, Valance, A, and Jenkins, JT (2017) The threshold for continuing saltation on Earth and other solar system bodies. *Journal of Geophysical Research: Earth Surface*. doi:10.1002/2016JF003982.

Burr, DM, Bridges, NT, Marshall, JR, Smith, JK, White, BR, and Emery, JP (2015) Higher-than-predicted saltation threshold wind speeds on Titan. *Nature*, **517**, 60–63. doi:10.1038/nature14088.

Chapman, S, and Cowling, TG (1970) *The mathematical theory of non-uniform gases The mathematical theory of non-uniform gases*, Vol. 27. doi:10.2307/3611062.

Charru, F, Andreotti, B, and Claudin, P (2013) Sand Ripples and Dunes. *Annual Review of Fluid Mechanics*, **45**(1), 469–493. doi:10.1146/annurev-fluid-011212-140806.

Charru, F, and Mouilleron-Arnould, H (2002) Instability of a bed of particles sheared by a viscous flow. *Journal of Fluid Mechanics*, **452**, 303–323. doi:10.1017/S0022112001006747.

Crassous, J, Beladjine, D, and Valance, A (2007) Impact of a Projectile on a Granular Medium Described by a Collision Model. *Physical Review Letters*, **99**(24), 248001. doi:10.1103/PhysRevLett.99.248001.

Creyssels, M, Dupont, P, El Moctar, a. O, … Rasmussen, KR (2009) Saltating particles in a turbulent boundary layer: experiment and theory. *Journal of Fluid Mechanics*, **625**, 47. doi:10.1017/S0022112008005491.

Cundall, PA;, and Strack, ODL (1979) A discrete numerical model for granular assemblies. *Geotechnique*, **29**(1), 47–65.

Dall'Acqua, D, Benucci, M, Corvaro, F, … Marchetti, B (2017) Experimental results of pipeline dewatering through surfactant injection. *Journal of Petroleum Science and Engineering*, **159**(September), 542–552. doi:10.1016/j.petrol.2017.08.068.

Durán, O, Andreotti, B, and Claudin, P (2012) Numerical simulation of turbulent sediment transport, from bed load to saltation. *Physics of Fluids (1994-Present)*, **24**, 103306. doi:10.1063/1.4757662.

Fernandez Luque, R, and Van Beek, R (1976) Erosion And Transport Of Bed-Load Sediment. *Journal of Hydraulic Research*, **14**(2), 127–144. doi:10.1080/00221687609499677.

Garzó, V, Tenneti, S, Subramaniam, S, and Hrenya, CM (2012) Enskog kinetic theory for monodisperse gas-solid flows. *Journal of Fluid Mechanics*, **712**, 129–168. doi:10.1017/jfm.2012.404.

Greeley, R, Iversen, J, Leach, R, Marshall, J, Williams, S, and White, B (1984) Windblown sand on Venus - Preliminary results of laboratory simulations. *Icarus*, **57**, 112–124. doi:10.1016/0019-1035(84)90013-7.

Guo, J, and Julien, PY (2007) Buffer law and transitional roughness effect in turbulent open-channel flows. In *The Fifth International Symposium on Environmental Hydraulics (ISEH V)*, , 1–6.

Ho, T-D (2012) *Etude expérimentale du transport de particules dans une couche limite turbulente*, Université de Rennes 1.

Iversen, JD, Pollack, JB, Greeley, R, and White, BR (1976) Saltation threshold on Mars: The effect of interparticle force, surface roughness, and low atmospheric density. *Icarus*, **29**(3), 381–393. doi:10.1016/0019-1035(76)90140-8.

Iversen, JD, and White, BR (1982) Saltation threshold on Earth, Mars and Venus. *Sedimentology*, **29**, 111–119. doi:10.1111/j.1365-3091.1982.tb01713.x.

Jenkins, J, Cantat, I, and Valance, A (2010) Continuum model for steady, fully developed saltation above a horizontal particle bed. *Physical Review E*, **82**, 020301. doi:10.1103/PhysRevE.82.020301.

Jenkins, J, and Hanes, D (1998) Collisional sheet flows of sediment driven by a turbulent fluid. *Journal of Fluid Mechanics*, **370**, 29–52. Retrieved from http://journals.cambridge.org/abstract_S0022112098001840

Jenkins, JT, and Valance, a. (2014) Periodic trajectories in aeolian sand transport. *Physics of Fluids*, **26**(7), 073301. doi:10.1063/1.4885576.

Jenkins, JT, and Valance, A (2018) Two-phase continuum theory for windblown sand. *Physical Review Fluids*, **3**(3), 34305. doi:10.1103/PhysRevFluids.3.034305.

Kok, JF, Parteli, EJR, Michaels, TI, and Karam, DB (2012) The physics of wind-blown sand and dust. *Reports on Progress in Physics*, **75**(10), 106901. doi:10.1088/0034-4885/75/10/106901.

Kok, JF, and Renno, NO (2009) A comprehensive numerical model of steady state saltation (COMSALT). *Journal of Geophysical Research: Atmospheres*, **114**(17), 1–20. doi:10.1029/2009JD011702.

Lämmel, M, Dzikowski, K, Kroy, K, Oger, L, and Valance, A (2017) Grain-scale modeling and splash parametrization for aeolian sand transport. *Physical Review E*, **95**(2). doi:10.1103/PhysRevE.95.022902.

Lämmel, M, Rings, D, and Kroy, K (2012) A two-species continuum model for aeolian sand transport. *New Journal of Physics*, **14**. doi:10.1088/1367-2630/14/9/093037.

Leporini, M, Terenzi, A, Marchetti, B, Corvaro, F, and Polonara, F (2019) On the numerical simulation of sand transport in liquid and multiphase pipelines. *Journal of Petroleum Science and Engineering*, **175**, 519–535. doi:10.1016/j.petrol.2018.12.057.

Niño, Y, and García, M (1998) Experiments on saltation of sand in water. *Journal of Hydraulic Engineering*, **124**(10), 1014–1025. doi:10.1061/(ASCE)0733-9429(1998)124:10(1014).

Oger, L, Ammi, M, Valance, A, and Beladjine, D (2005) Discrete Element Method studies of the collision of one rapid sphere on 2D and 3D packings. *The European Physical Journal E*, **17**(4), 467–76. doi:10.1140/epje/i2005-10022-x.

Ouriemi, M, Aussillous, P, and Guazzelli, É (2009) Sediment dynamics. Part 1. Bed-load transport by laminar shearing flows. *Journal of Fluid Mechanics*, **636**, 295. doi:10.1017/S0022112009007915.

Owen, PR (1964) Saltation of uniform grains in air. *Journal of Fluid Mechanics*, **20**(2), 225–242.

Pähtz, T, Clark, AH, Valyrakis, M, and Durán, O (2020) The Physics of Sediment Transport Initiation, Cessation, and Entrainment Across Aeolian and Fluvial Environments. *Reviews of Geophysics*, **58**(1). doi:10.1029/2019RG000679.

Pähtz, T, and Durán, O (2020a) Unification of Aeolian and Fluvial Sediment Transport Rate from Granular Physics. *Physical Review Letters*, **124**, 168001. doi:10.1103/physrevlett.124.168001.

Pähtz, T, and Durán, O (2020b) Unification of Aeolian and Fluvial Sediment Transport Rate from Granular Physics - Supplemental Material. *Physical Review Letters*. doi:10.1103/physrevlett.124.168001.

Pähtz, T, Durán, O, Ho, T, Valance, A, and Kok, JF (2015) The fluctuation energy balance in non-suspended fluid-mediated particle transport. *Physics of Fluids*, **27**, 013303. doi:10.1063/1.4905911.

Pähtz, T, Kok, JF, and Herrmann, HJ (2012) The apparent roughness of a sand surface blown by wind from an analytical model of saltation. *New Journal of Physics*, **14**(September 2016). doi:10.1088/1367-2630/14/4/043035.

Pasini, JM, and Jenkins, JT (2005) Aeolian transport with collisional suspension. *Philosophical Transactions. Series A, Mathematical, Physical, and Engineering Sciences*, **363**(1832), 1625–46. doi:10.1098/rsta.2005.1598.

Ralaiarisoa, JL, Besnard, JB, Furieri, B, … Valance, A (2020) Transition from Saltation to Collisional Regime in Windblown Sand. *Physical Review Letters*, **124**(19), 198501. doi:10.1103/PhysRevLett.124.198501.

Saha, S, and Alam, M (2016) Normal stress differences , their origin and constitutive relations for a sheared granular fluid. *J. Fluid Mech*, **795**, 549–580. doi:10.1017/jfm.2016.237.

Saha, S, and Alam, M (2017) Revisiting ignited-quenched transition and the non-Newtonian rheology of a sheared dilute gas-solid suspension. *Journal of Fluid Mechanics*, **833**, 206–246. doi:10.1017/jfm.2017.722.

Sauermann, G, Kroy, K, and Herrmann, HJ (2001) A Continuum Saltation Model for Sand Dunes. *Physical Review E*, **64**, 031305. doi:10.1103/PhysRevE.64.031305.

Seizilles, G, Lajeuness, E, Devauchelle, O, and Bak, M (2014) Cross-stream diffusion in bedload transport. *Phys. Fluids*, **26**, 013302. doi:10.1063/1.4861001.

Tholen, K, Pähtz, T, Kamath, S, Parteli, EJR, and Kroy, K (2023) Anomalous Scaling of Aeolian Sand Transport Reveals Coupling to Bed Rheology. *Physical Review Letters*, **130**(5), 58204. doi:10.1103/PhysRevLett.130.058204.

Tsuji, Y, Kawaguchi, T, and Tanaka, T (1993) Discrete particle simulation of two-dimensional fluidized bed. *Powder Technology*, **77**(1), 79–87.

Valance, A, and Berzi, D (2022) Particle saltation over rigid bumpy beds in viscous shearing flows. *Journal of Fluid Mechanics*, **947**, 1–28. doi:10.1017/jfm.2022.616.

Valance, A, Rasmussen, KR, Ould El Moctar, A, and Dupont, P (2015) The physics of Aeolian sand transport. *Comptes Rendus Physique*, **16**(1), 105–117. doi:10.1016/j.crhy.2015.01.006.

Werner, B (1990) A steady-state model of wind-blown sand transport. *The Journal of Geology*, **98**(1), 1–17. Retrieved from http://www.jstor.org/stable/30068220

Appendix A. Approximate analytical trajectories for the saltating particles

We characterize the drag exerted on the particles through a drag coefficient, C_D, that we take to be independent of y, as in Pasini and Jenkins (2005), to obtain analytical expressions for the particle trajectories.

Integrating the vertical momentum balance for the particle:

$$\frac{\mathrm{d}\xi_y}{\mathrm{d}t} + C_D\xi_y + 1 = 0, \tag{A1}$$

with ξ_y the vertical component of the particle velocity, we obtain the vertical velocity at any time t after the particle reaches a certain ascending velocity ξ_y^+ at a certain location y_r,

$$\xi_y = \frac{C_D\xi_y^+ + 1 - \exp\left(C_D t\right)}{C_D \exp\left(C_D t\right)}; \tag{A2}$$

and, with another integration, the position y as a function of time,

$$y - y_r = \frac{\left(C_D\xi_y^+ + 1\right)\left[1 - \exp\left(-C_D t\right)\right] - C_D t}{C_D{}^2}. \tag{A3}$$

From equation (A3) we obtain an implicit expression for the time that the particle spends at $y \geq y_r$

$$t_f = \frac{C_D\xi_y^+ + 1}{C_D}\left[1 - \exp\left(-C_D t_f\right)\right]. \tag{A4}$$

Then, from equation (A2), with $t = t_f$, the downward vertical velocity of the particle at $y = y_r$ is

$$\xi_y{}^- = \xi_y^+ - t_f. \tag{A5}$$

To permit subsequent analytical integrations, we propose the following explicit expression for the time of flight,

$$t_f = \xi_y^+ + \frac{1}{C_D} - \frac{1}{C_D}\exp\left(-C_D\xi_y^+\right), \tag{A6}$$

which has the right limits at both small $C_D\xi_y^+$, i.e., $t_f = 2\xi_y^+$, and large $C_D\xi_y^+$, i.e., $t_f = \xi_y^+ + C_D{}^{-1}$. With this, equation (A5) gives

$$\xi_y^- = -\frac{1}{C_D} + \frac{1}{C_D}\exp\left(-C_D\xi_y^+\right). \tag{A7}$$

In the limit of large $C_D\xi_y^+$, equation (A7) reduces to

$$\xi_y^- = -\frac{1}{C_D}. \tag{A8}$$

We next integrate the horizontal particle momentum balances, and distinguish between saltation in viscous and in turbulent shearing flows.

A1. Saltation in viscous shearing flows

In the case of saltation in viscous shearing flows, we assume that the fluid velocity profile is locally linear (that is for $y \geq y_r$), so that the horizontal momentum balance for the particles is:

$$\frac{\mathrm{d}\xi_x}{\mathrm{d}t} = C_D\left[U + \frac{\mathrm{d}U}{\mathrm{d}y}\left(y - y_r\right) - \xi_x\right], \tag{A9}$$

with ξ_x the horizontal component of the particle velocity, and U and $\frac{\mathrm{d}U}{\mathrm{d}y}$ the fluid horizontal velocity and shear rate at the reference level. In the following integrations, we treat $\frac{\mathrm{d}U}{\mathrm{d}y}$ for saltation in viscous shearing flows as if it were constant. Then, after inserting equation (A3) into equation (A9), and integrating with the initial condition $\xi_x(t = 0) = \xi_x^+$,

$$\begin{aligned}\xi_x = U + \frac{\mathrm{d}U}{\mathrm{d}y}\frac{\left(C_D\xi_y^+ + 1\right)}{{C_D}^2}\left[1 - C_D t\exp\left(-C_D t\right) - \exp\left(-C_D t\right)\right] \\ - \frac{\mathrm{d}U}{\mathrm{d}y}\frac{C_D t - 1 + \exp\left(-C_D t\right)}{{C_D}^2} + \left(\xi_x^+ - U\right)\exp\left(-C_D t\right).\end{aligned} \tag{A10}$$

The horizontal velocity after the time t_f is, then, with equations (A4) and (A6),

$$\begin{aligned}\xi_x^- = U + \frac{1}{{C_D}^2}\frac{\mathrm{d}U}{\mathrm{d}y}\frac{1}{C_D\xi_y^+ + 1}\left[C_D\xi_y^+ + 1 - \exp\left(-C_D\xi_y^+\right)\right]\left[1 - \exp\left(-C_D\xi_y^+\right) - C_D\xi_y^+\exp\left(-C_D\xi_y^+\right)\right] \\ + \frac{\xi_x^+ - U}{C_D\xi_y^+ + 1}\exp\left(-C_D\xi_y^+\right),\end{aligned} \tag{A11}$$

In the limit of large $C_D\xi_y^+$, equation (A11) gives

$$\xi_x^- = U + \frac{1}{{C_D}^2}\frac{\mathrm{d}U}{\mathrm{d}y}. \tag{A12}$$

Equation (A10) can be integrated with the boundary condition $x(t = 0) = x_i$ to obtain the horizontal displacement from the initial position at the reference level as a function of time:

$$\begin{aligned}x = x_i + Ut + \frac{\left(C_D\xi_y^+ + 1\right)}{{C_D}^2}\frac{\mathrm{d}U}{\mathrm{d}y}\left[\exp\left(-C_D t\right)\left(\frac{2}{C_D} + t\right) + t - \frac{2}{C_D}\right] \\ - \frac{1}{{C_D}^2}\frac{\mathrm{d}U}{\mathrm{d}y}\left[\frac{C_D t^2}{2} - t - \frac{1}{C_D}\exp\left(-C_D t\right) + \frac{1}{C_D}\right] + \frac{1}{C_D}\left(\xi_x^+ - U\right)\left[1 - \exp\left(-C_D t\right)\right].\end{aligned} \tag{A13}$$

The horizontal displacement Δ after the time t_f is

$$\begin{aligned}\Delta = Ut_f + \frac{\left(C_D\xi_y^+ + 1\right)}{{C_D}^2}\frac{\mathrm{d}U}{\mathrm{d}y}\left[\exp\left(-C_D t_f\right)\left(\frac{2}{C_D} + t_f\right) + t_f - \frac{2}{C_D}\right] \\ - \frac{1}{{C_D}^2}\frac{\mathrm{d}U}{\mathrm{d}y}\left[\frac{C_D {t_f}^2}{2} - t_f - \frac{1}{C_D}\exp\left(-C_D t_f\right) + \frac{1}{C_D}\right] + \frac{1}{C_D}\left(\xi_x^+ - U\right)\left[1 - \exp\left(-C_D t_f\right)\right].\end{aligned} \tag{A14}$$

In the limit of large $C_D\xi_y^+$, $t_f = \xi_y^+ + {C_D}^{-1}$ and equation (A14) reduces to

$$\Delta = \frac{1}{2C_D}\frac{\mathrm{d}U}{\mathrm{d}y}\xi_y^{+2} + U\xi_y^{+} + \frac{\xi_x^{+} - U}{C_D}. \tag{A15}$$

A2. Saltation in turbulent shearing flows

In the case of saltation in turbulent shearing flows, we assume that the fluid velocity is equal to its average, $\bar{U}$, in the region between the reference location y_r and the top of the trajectory, y_M, determined from equation (A3) at the time t for which ξ_y in equation (A2) vanishes. Then, the horizontal momentum balance for the particles reads:

$$\frac{\mathrm{d}\xi_x}{\mathrm{d}t} = C_D\left(\bar{U} - \xi_x\right) \tag{A16}$$

where, with the expression for the turbulent fluid shear stress,

$$\begin{aligned}
\bar{U} &= \frac{1}{y_M - y_r}\int_{y_r}^{y_M} U + \frac{\sqrt{rS}}{\kappa}\ln\left(1 + \frac{y - y_r}{y_r + y_0}\right)\mathrm{d}y \\
&= U + \frac{\sqrt{rS}}{\kappa}\left[\left(1 + \frac{y_r + y_0}{y_M - y_r}\right)\ln\left(\frac{y_M - y_r}{y_r + y_0} + 1\right) - 1\right] \\
&= U + \frac{\sqrt{rS}}{\kappa}\left[\left(1 + {C_D}^2\frac{y_r + y_0}{C_D\xi_y^{+} - \ln\left(C_D\xi_y^{+} + 1\right)}\right)\ln\left(\frac{1}{{C_D}^2}\frac{C_D\xi_y^{+} - \ln\left(C_D\xi_y^{+} + 1\right)}{y_r + y_0} + 1\right) - 1\right] \\
&\approx U + 0.85\frac{\sqrt{rS}}{\kappa}\ln\left(\frac{1}{C_D}\frac{\xi_y^{+}}{y_r + y_0} + 1\right) = U + 0.85\frac{\sqrt{rS}}{\kappa}\ln\left(\frac{\kappa\xi_y^{+}}{C_D\sqrt{rS}}\frac{\mathrm{d}U}{\mathrm{d}y} + 1\right),
\end{aligned} \tag{A17}$$

with U and $\frac{\mathrm{d}U}{\mathrm{d}y}$ the fluid horizontal velocity and shear rate at the reference level . In equation (A17), we have taken the limit of large $C_D\xi_y^{+}$ to approximate the average fluid velocity. The factor 0.85 in front of the logarithm allows to better fit the trajectories of discrete-continuum simulations of saltation in turbulent shearing flows.

Then, after integrating equation (A16) with the initial condition $\xi_x(t = 0) = \xi_x^{+}$,

$$\xi_x = \bar{U}\left[1 - \exp\left(-C_D t\right)\right] + \xi_x^{+}\exp\left(-C_D t\right). \tag{A18}$$

The horizontal velocity after the time t_f is, then, with equations (A5) and (A7),

$$\xi_x^{-} = \bar{U}\left[1 - \frac{\exp\left(-C_D\xi_y^{+}\right)}{C_D\xi_y^{+} + 1}\right] + \frac{\xi_x^{+}}{C_D\xi_y^{+} + 1}\exp\left(-C_D\xi_y^{+}\right). \tag{A19}$$

In the limit of large $C_D\xi_y^{+}$, equation (A19) gives

$$\xi_x^{-} = \bar{U}. \tag{A20}$$

Equation (A18) can be integrated with the boundary condition $x(t = 0) = x_i$ to obtain the horizontal displacement from the initial position at the reference level as a function of time:

$$x = x_i + \bar{U}t + \frac{1}{C_D}\left[\xi_x^{+} - \bar{U}\right]\left[1 - \exp\left(-C_D t\right)\right]. \quad \text{(A21)}$$

The horizontal displacement Δ after the time t_f is

$$\Delta = \bar{U}t_f + \frac{1}{C_D}\left[\xi_x^{+} - \bar{U}\right]\left[1 - \exp\left(-C_D t_f\right)\right]. \quad \text{(A22)}$$

In the limit of large $C_D\xi_y^{+}$, $t_f = \xi_y^{+} + C_D^{-1}$ and equation (A22) reduces to

$$\Delta = \bar{U}\xi_y^{+} + \frac{\xi_x^{+}}{C_D}. \quad \text{(A23)}$$

Appendix B. Constitutive relations

We define the average of a certain quantity φ at a certain distance *y* from the bed as:

$$\langle\varphi\rangle = \frac{\pi}{6c}\int_{all\,\xi}\varphi f \mathrm{d}^2\boldsymbol{\xi} = \frac{\pi}{6c}\int_{all\,\xi^+}\varphi^+ f^+ \mathrm{d}^2\boldsymbol{\xi}^+ + \frac{\pi}{6c}\int_{all\,\xi^-}\varphi^- f^- \mathrm{d}^2\boldsymbol{\xi}^- \tag{B1}$$

where *f* is the velocity distribution of particles at that height and 6c/π is the number density. As in Creyssels et al. (2009), we distinguish between ascending or descending particles and introduce velocity distributions for both species. We assume that the velocity distribution of the ascending particles is an anisotropic Maxwellian:

$$f^+ = \frac{6}{\pi}\frac{c^+}{\pi\sqrt{T_x^+ T_y^+}}\exp\left[-\frac{\left(\xi_x^+ - u\right)^2}{2T_x^+}\right]\exp\left(-\frac{\xi_y^{+2}}{2T_y^+}\right), \tag{B2}$$

where: $u = \langle\xi_x\rangle$; and $T_x^+ = \frac{\pi}{6c^+}\int_{all\,\xi^+}\left(\xi_x^+ - u\right)^2 f^+ \mathrm{d}^2\boldsymbol{\xi}^+$ and $T_y^+ = \frac{\pi}{6c^+}\int_{all\,\xi^+}\xi_y^{+2} f^+ \mathrm{d}^2\boldsymbol{\xi}^+$ are the mean squares of the horizontal velocity fluctuations of the ascending particles. The concentration of the ascending particles, c^+, is equal to $\frac{\pi}{6}\int_{all\,\xi^+} f^+ \mathrm{d}^2\boldsymbol{\xi}^+$, while that of the descending particle is $c^- = \frac{\pi}{6}\int_{all\,\xi^-} f^- \mathrm{d}^2\boldsymbol{\xi}^-$. When $\varphi = 1$, equation (B1) gives $c = c^+ + c^-$.

Given that we are dealing with steady states, $\langle\xi_y\rangle = 0$, so that

$$\langle\xi_y\rangle = \frac{\pi}{6c}\int_{all\,\xi^+}\xi_y^+ f^+ \mathrm{d}^2\boldsymbol{\xi}^+ + \frac{\pi}{6c}\int_{all\,\xi^-}\xi_y^- f^- \mathrm{d}^2\boldsymbol{\xi}^- = 0. \tag{B3}$$

Then, we take the limit for large $C_D\xi_y^+$ of ξ_y^- (equation A9) and, inserting equation (B2) into equation (B3), and integrating, we obtain

$$\begin{aligned}
&\frac{c^+}{\pi\sqrt{T_x^+ T_y^+}}\int_0^{+\infty}\xi_y^+\exp\left(-\frac{\xi_y^{+2}}{2T_y^+}\right)\int_{-\infty}^{+\infty}\exp\left[-\frac{\left(\xi_x^+ - u\right)^2}{2T_x^+}\right]\mathrm{d}\xi_x^+\mathrm{d}\xi_y^+ = -\frac{\pi}{6}\int_{all\,\xi^-}\xi_y^- f^- d^2\boldsymbol{\xi}^- \\
&\frac{c^+\sqrt{2}}{\sqrt{\pi T_y^+}}\int_0^{+\infty}\xi_y^+\exp\left(-\frac{\xi_y^{+2}}{2T_y^+}\right)\mathrm{d}\xi_y^+ = \frac{1}{C_D}\frac{\pi}{6}\int_{all\,\xi^-} f^- \mathrm{d}^2\boldsymbol{\xi}^- \\
&c^+ C_D\sqrt{\frac{2T_y^+}{\pi}} = c^-,
\end{aligned} \tag{B4}$$

that is a relation between the concentrations of the two species of particles. As shown later, we found that equation (B4) does not correctly capture the right limit as T_y^+ tends to zero, and also slightly underestimates c^-. An almost perfect agreement can be obtained, instead, with

$$c^- = c^+ + \frac{3}{4}c^+ C_D\sqrt{\frac{2T_y^+}{\pi}}. \tag{B5}$$

From this and the definition of *c*,

$$c = c^+ + c^- = c^+\left(2+\frac{3}{4}C_D\sqrt{\frac{2T_y^+}{\pi}}\right). \tag{B6}$$

Taking the limit for large $C_D\xi_y^+$ permits equations (B4)-(B6) to be obtained without assuming a velocity distribution for the descending particles. We show the comparisons between equations (B5) and (B6) and the results of numerical simulations on saltation of particles in a viscous shearing flow experiencing Stokes drag in figure B1.

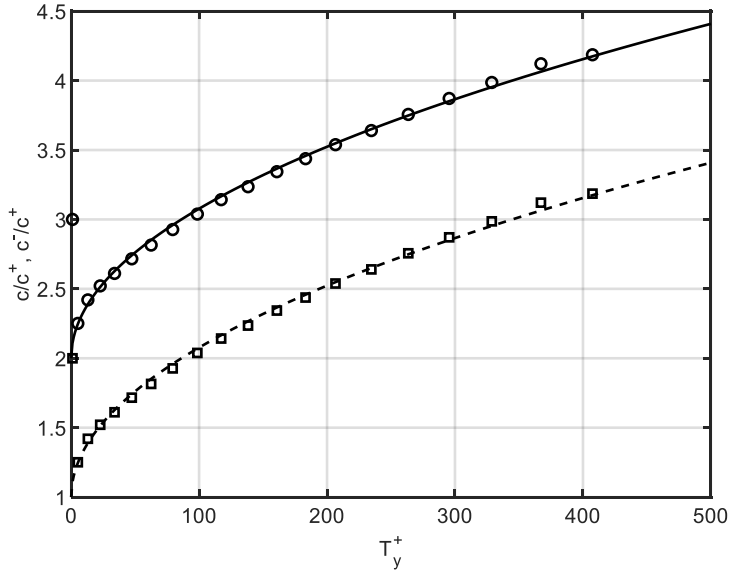

Fig. B1. Concentration ratios c/c^+ (circles) and c^-/c^+ (squares) as functions of T_y^+ measured in numerical simulations of saltation in a viscous shearing flow with d_w = 1, St = 100, r = 150000, Sh = 0.05 (so that the Stokes drag is dominant and C_D = 18/St = 0.18) and M = 0.0131. The dashed and solid lines are the predictions of equations (B5) and (B6), respectively.

Equation (B1) can be rewritten as

$$\begin{aligned}\langle\varphi\rangle &= \frac{\pi}{6c}\int_{all\,\xi^+}\varphi^+ f^+ \mathrm{d}^2\boldsymbol{\xi}^+ + \frac{\pi}{6c}\int_{all\,\xi^-}\varphi^- f^- \mathrm{d}^2\boldsymbol{\xi}^- = \frac{\pi}{6c}\int_{all\,\xi^+}\varphi^+ f^+ \mathrm{d}^2\boldsymbol{\xi}^+ + \frac{\pi}{6c}\int_{all\,\xi^+}\varphi^- f^- \left|J^-\right| \mathrm{d}^2\boldsymbol{\xi}^+ \\ &= \frac{\pi}{6c}\int_{all\,\xi^+}\left[\varphi^+ f^+ + \varphi^- f^- \left|J^-\right|\right]\mathrm{d}^2\boldsymbol{\xi}^+,\end{aligned} \tag{B7}$$

where J^- is the Jacobian of the transformation from $\boldsymbol{\xi}^+$ into $\boldsymbol{\xi}^-$. When we calculate the average vertical flux of the generic quantity,

$$\left\langle\varphi\xi_y\right\rangle = \frac{\pi}{6c}\int_{all\,\xi^+}\left[\varphi^+\xi_y{}^+ f^+ + \varphi^-\xi_y{}^- f^- \left|J^-\right|\right]\mathrm{d}^2\boldsymbol{\xi}^+ = \frac{\pi}{6c}\int_{all\,\xi^+}\left[\varphi^+ - \varphi^-\right]\xi_y{}^+ f^+ \mathrm{d}^2\boldsymbol{\xi}^+, \tag{B8}$$

where we made use of the fact that, at steady state, $\left\langle\xi_y\right\rangle = 0$ and, therefore, from equation (B3), if the trajectories are independent of each other (that is for small mass hold-ups), $\xi_y{}^+ f^+ = -\xi_y{}^- f^- \left|J^-\right|$ (Pasini and Jenkins 2005).

The particle normal stress in the *y*-direction, in the absence of particle interaction, is simply given by the average vertical flux of *y*-momentum, $\sigma_y \equiv c\left\langle \xi_y \xi_y \right\rangle = cT_y$, where $T_y = \left\langle \xi_y{}^2 \right\rangle$ is the mean square of the vertical velocity fluctuation for all the particles. However, using equation (B8),

$$\sigma_y = \frac{\pi}{6}\int_0^{+\infty}\int_{-\infty}^{+\infty}\left(\xi_y{}^+ - \xi_y{}^-\right)\xi_y{}^+ f^+ \mathrm{d}\xi_x{}^+ \mathrm{d}\xi_y{}^+. \tag{B9}$$

Then, upon taking the limit for large $C_D\xi_y^+$ of ξ_y^- (equation A9) and, inserting equation (B2) into equation (B9), and integrating, we obtain

$$\begin{aligned}\sigma_y &= \frac{c^+}{\pi\sqrt{T_x{}^+ T_y{}^+}}\int_0^{+\infty}\left(\xi_y{}^+ + \frac{1}{C_D}\right)\xi_y{}^+ \exp\left(-\frac{\xi_y{}^{+2}}{2T_y{}^+}\right)\int_{-\infty}^{+\infty}\exp\left[-\frac{\left(\xi_x{}^+ - u\right)^2}{2T_x{}^+}\right]\mathrm{d}\xi_x{}^+\mathrm{d}\xi_y{}^+ \\ &= \frac{c^+}{\pi\sqrt{T_x{}^+ T_y{}^+}}\sqrt{2\pi T_x{}^+}\int_0^{+\infty}\left(\xi_y{}^+ + \frac{1}{C_D}\right)\xi_y{}^+ \exp\left(-\frac{\xi_y{}^{+2}}{2T_y{}^+}\right)\mathrm{d}\xi_y{}^+ = c^+T_y{}^+ + c^+\frac{1}{C_D}\sqrt{\frac{2T_y{}^+}{\pi}}.\end{aligned} \tag{B10}$$

The limit for large $C_D\xi_y^+$ permits a simple expression for σ_y (and for the other constitutive relations) to be obtained. This approximation is valid whenever the Maxwellian vertical velocity distribution of the ascending particles is wide, that is for large T_y^+, so that the contribution of the large ξ_y^+ is significant. Conversely, it becomes less accurate near the top of the saltating layer, where we expect small values of T_y^+ and a subsequent narrower distribution of ξ_y^+ around zero. If we use the more accurate equation (A7) in equation (B9), we would obtain the following constitutive relation for the particle normal stress:

$$\begin{aligned}\sigma_y &= \frac{c^+}{\pi\sqrt{T_x{}^+ T_y{}^+}}\int_0^{+\infty}\left(\xi_y{}^+ + \frac{1}{C_D} - \frac{1}{C_D}\exp\left(-C_D\xi_y^+\right)\right)\xi_y{}^+ \exp\left(-\frac{\xi_y{}^{+2}}{2T_y{}^+}\right)\int_{-\infty}^{+\infty}\exp\left[-\frac{\left(\xi_x{}^+ - u\right)^2}{2T_x{}^+}\right]\mathrm{d}\xi_x{}^+\mathrm{d}\xi_y{}^+ \\ &= \frac{c^+}{\pi\sqrt{T_x{}^+ T_y{}^+}}\sqrt{2\pi T_x{}^+}\int_0^{+\infty}\left(\xi_y{}^+ + \frac{1}{C_D} - \frac{1}{C_D}\exp\left(-C_D\xi_y^+\right)\right)\xi_y{}^+ \exp\left(-\frac{\xi_y{}^{+2}}{2T_y{}^+}\right)\mathrm{d}\xi_y{}^+ \\ &= c^+T_y{}^+ + c^+T_y{}^+\exp\left(\frac{C_D{}^2T_y{}^+}{2}\right)\mathrm{erfc}\left(\sqrt{\frac{C_D{}^2T_y{}^+}{2}}\right).\end{aligned} \tag{B11}$$

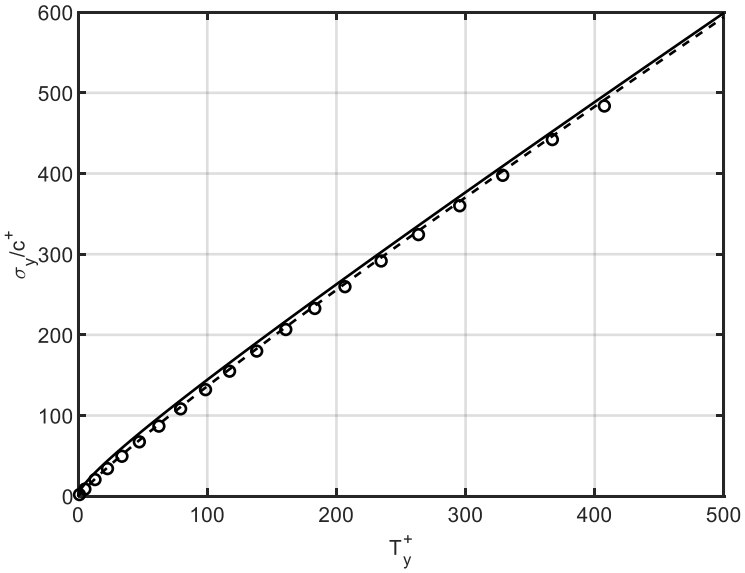

Fig. B2. Ratio of particle normal stress over particle concentration of ascending particles as a function of T_y^+ measured in numerical simulations of saltation in a viscous shearing flow with $d_w = 1$, St = 100, $r = 150000$, Sh = 0.05 (so that the Stokes drag is dominant and $C_D = 18/\mathrm{St} = 0.18$) and $M = 0.0131$. The solid and dashed lines are the predictions of equations (B10) and (B11), respectively.

The difference between the approximate equation (B10) and the more accurate equation (B11) is shown in figure B2 when the drag coefficient is equal to 0.18, and we notice that the mismatch becomes relevant only at small T_y^+, as expected. The agreement with the measurements in the numerical simulations of saltation of particles in a viscous shearing flow experiencing Stokes drag is remarkable.

From $\sigma_y = cT_y$, equations (B10) and (B6), we obtain

$$T_y = \frac{4\sqrt{\pi}C_D T_y^+ + 4\sqrt{2T_y^+}}{8\sqrt{\pi}C_D + 3{C_D}^2\sqrt{2T_y^+}}; \tag{B12}$$

while, with equation (A10),

$$T_y^- = \frac{\pi}{6c^-}\int_{all\ \xi^-}\left(\xi_y^-\right)^2 f^- \mathrm{d}^2\boldsymbol{\xi}^- = \frac{1}{{C_D}^2}. \tag{B13}$$

We show the agreement between equations (B12) and (B13) and the measurements in the numerical simulations of saltation of particles in a viscous shearing flow experiencing Stokes drag in figure B3.

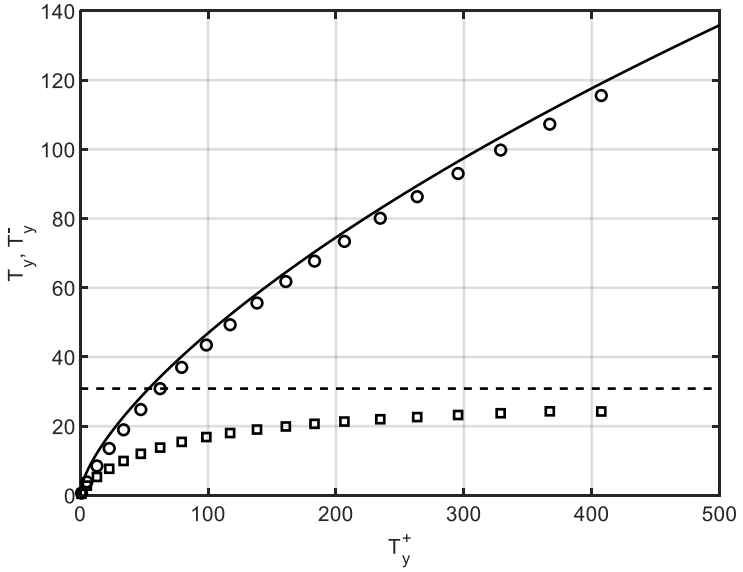

Fig. B3. T_y (circles) and T_y^- (squares) as functions of T_y^+ measured in numerical simulations of saltation in a viscous shearing flow d_w = 1, St = 100, r = 150000, Sh = 0.05 (so that the Stokes drag is dominant and C_D = 18/St = 0.18) and M = 0.0131. The solid and dashed lines are the predictions of equations (B12) and (B13), respectively.

The *yyy*-element of the vertical flux of the particle second moment is $Q_{yyy} \equiv c\left\langle \xi_y \xi_y \xi_y \right\rangle$, so that, with equation (B8),

$$Q_{yyy} = \frac{\pi}{6}\int_0^{+\infty}\int_{-\infty}^{+\infty}\left(\xi_y^{+2} - \xi_y^{-2}\right)\xi_y^{+} f^{+}\mathrm{d}\xi_x^{+}\mathrm{d}\xi_y^{+}. \tag{B14}$$

Then, In the limit of large $C_D\xi_y^+$, upon using equations (A8) and (B2) in equation (B14), and integrating,

$$\begin{aligned} Q_{yyy} &= \frac{c^+}{\pi\sqrt{T_x^+ T_y^+}}\int_0^{+\infty}\int_{-\infty}^{+\infty}\left(\xi_y^{+2} - \frac{1}{C_D{}^2}\right)\xi_y^{+}\exp\left[-\frac{\left(\xi_x^{+}-u\right)^2}{2T_x^+}\right]\exp\left(-\frac{\xi_y^{+2}}{2T_y^+}\right)\mathrm{d}\xi_x^{+}\mathrm{d}\xi_y^{+} \\ &= \frac{c^+}{\pi\sqrt{T_x^+ T_y^+}}\sqrt{2\pi T_x^+}\int_0^{+\infty}\left(\xi_y^{+3} - \frac{1}{C_D{}^2}\xi_y^{+}\right)\exp\left(-\frac{\xi_y^{+2}}{2T_y^+}\right)\mathrm{d}\xi_y^{+} = c^+\sqrt{\frac{2T_y^+}{\pi}}\left(2T_y^{+} - \frac{1}{C_D{}^2}\right). \end{aligned} \tag{B15}$$

An undesirable, non-physical consequence of equation (B15) is that Q_{yyy} vanishes at a finite, nonzero value of T_y^+. However, in the same limit of large $C_D\xi_y^+$, we can ignore the second term between brackets and obtain

$$Q_{yyy} = \sqrt{\frac{8}{\pi}}c^{+}T_y^{+3/2}. \tag{B16}$$

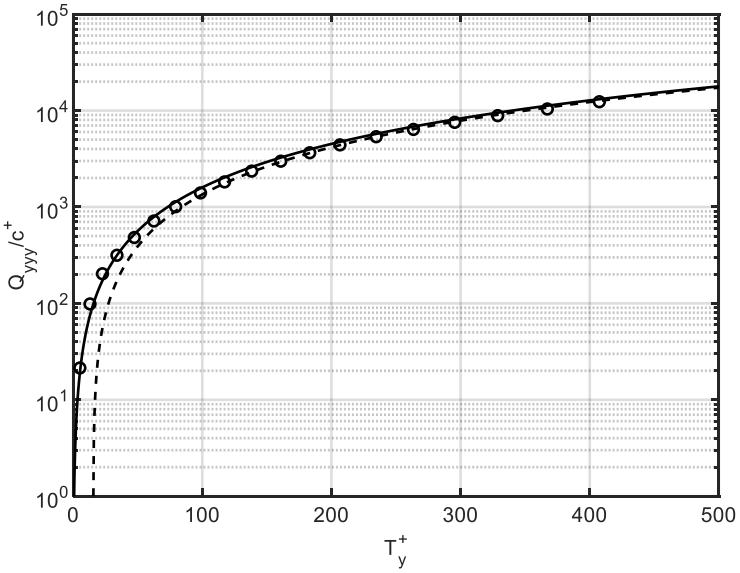

Fig. B4. Ratio of energy flux Q_{yyy} over particle concentration of ascending particles as a function of T_y^+ measured in numerical simulations of saltation in a viscous shearing flow with d_w = 1, St = 100, r = 150000, Sh = 0.05 (so that the Stokes drag is dominant and C_D = 18/St = 0.18) and M = 0.0131. The dashed and solid lines are the predictions of equations (B15) and (B16), respectively.

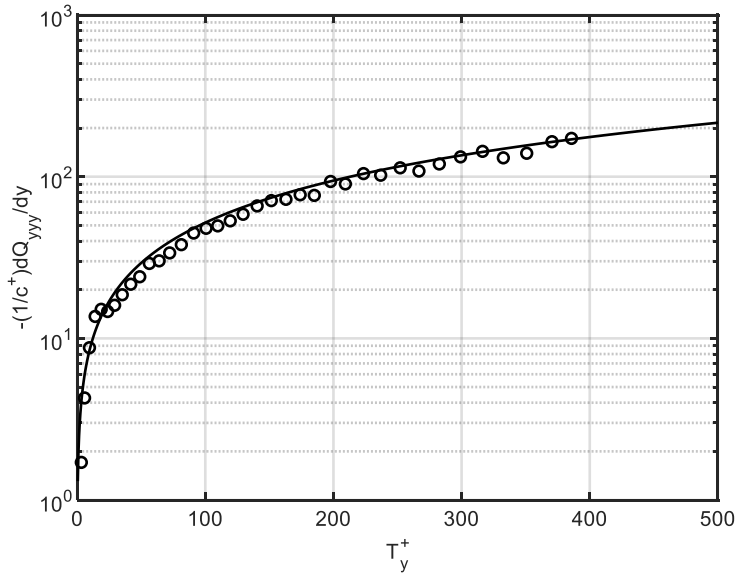

Fig. B5. Negative of the derivative of Q_{yyy} over particle concentration of ascending particles as a function of T_y^+ measured in numerical simulations of saltation in a viscous shearing flow with d_w = 1, St = 100, r = 150000, Sh = 0.05 (so that the Stokes drag is dominant and C_D = 18/St = 0.18) and M = 0.0131. The solid line is the predictions of D_{yy}/c^+ from equations (B17).

Figure B4 indicates that the predictions of equations (B15) and (B16) are in excellent agreement with the measurements in numerical simulations of saltation of particles in a viscous shearing flow experiencing Stokes drag, but only equation (B16) has the correct limit for vanishing T_y^+.

The *yy*-element of the dissipation tensor due to fluid drag in the balance of particle second moment is $D_{yy} \equiv 2cC_D \left\langle \xi_y \xi_y \right\rangle$ (Saha and Alam 2017), so that, with the definition of σ_y and equation (B10),

$$D_{yy} = 2C_D\sigma_y = 2C_D c^+ T_y^+ + 2c^+\sqrt{\frac{2T_y^+}{\pi}}. \tag{B17}$$

Equation (9) indicates that D_{yy} should be equal to the negative of the derivative of Q_{yyy}. Figure B5 shows that the values of $-\frac{1}{c^+}\frac{\mathrm{d}Q_{yyy}}{\mathrm{d}y}$ measured in numerical simulations of saltation of particles in a viscous shearing flow experiencing Stokes drag as a function of T_y^+ do indeed match the predictions of D_{yy}/c^+ from equation (B17).

Finally, the particle shear stress is equal to the negative of the average vertical flux of *x*-momentum, $s \equiv -c\left\langle \xi_x \xi_y \right\rangle$, so that, from equation (B8),

$$s = -\frac{\pi}{6}\int_0^{+\infty}\int_{-\infty}^{+\infty}\left(\xi_x^+ - \xi_x^-\right)\xi_y^+ f^+ \mathrm{d}\xi_x^+ \mathrm{d}\xi_y^+. \tag{B18}$$

To proceed, we must distinguish between saltation in viscous and turbulent shearing flows, because of the influence of the fluid velocity on the particle horizontal velocity.

B1. Saltation in viscous shearing flows

In the limit of large $C_D\xi_y^+$, using equations (A12) and (B2) into equation (B18), and integrating, we obtain the following expression, in the case of saltation in viscous shearing flows,

$$\begin{aligned} s &= -\frac{c^+}{\pi\sqrt{T_x^+ T_y^+}}\int_0^{+\infty}\xi_y^+ \exp\left(-\frac{\xi_y^{+2}}{2T_y^+}\right)\int_{-\infty}^{+\infty}\left[\left(\xi_x^+ - u\right) + u - U - \frac{1}{{C_D}^2}\frac{\mathrm{d}U}{dy}\right]\exp\left[-\frac{\left(\xi_x^+ - u\right)^2}{2T_x^+}\right]\mathrm{d}\xi_x^+ \mathrm{d}\xi_y^+ \\ &= \frac{c^+}{\pi\sqrt{T_x^+ T_y^+}}\sqrt{\pi 2T_x^+}\left(U - u + \frac{1}{{C_D}^2}\frac{\mathrm{d}U}{\mathrm{d}y}\right)\int_0^{+\infty}\xi_y^+ \exp\left(-\frac{\xi_y^{+2}}{2T_y^+}\right)d\xi_y^+ \\ &= c^+\sqrt{\frac{2T_y^+}{\pi}}\left(U - u + \frac{1}{{C_D}^2}\frac{\mathrm{d}U}{\mathrm{d}y}\right). \end{aligned} \tag{B19}$$

Equation (B19) indicates that there is no influence of T_x^+ on the shear stress, because of the assumed Gaussian distribution of ξ_x^+ that causes the term involving (ξ_x^+-*u*) in the integrand of equation (B15) to disappear. However, (Valance and Berzi 2022) showed that the PDF of the downward velocity of the particles impacting the bed (dominated by the horizontal component) is actually non-symmetric. Given the perfect agreement with respect to the other constitutive relations obtained in this Appendix, which do not involve the horizontal velocity of the ascending particles, we are inclined to ascribe to the non-symmetric distribution of ξ_x^+ the fact that the shear stress measured in simulations of saltation particles in a viscous shearing flow experiencing Stokes drag (figure B6a) is not linear in the velocity difference, *U*-*u*, as implied by equation (B19). At small T_y^+, equation (B10) in equation (B19) actually indicates that $s \propto C_D\sigma_y\left(U - u + \frac{1}{{C_D}^2}\frac{\mathrm{d}U}{\mathrm{d}y}\right)$. We found that

$$s = \frac{3}{5}C_D\sigma_y\left(U - u + \frac{2}{3}\frac{1}{{C_D}^2}\frac{\mathrm{d}U}{\mathrm{d}y}\right) \tag{B20}$$

permits to reproduce the behaviour of the particle shear stress for saltation in viscous shearing flows better than equation (B19) in almost the entire flow domain (figure B6b).

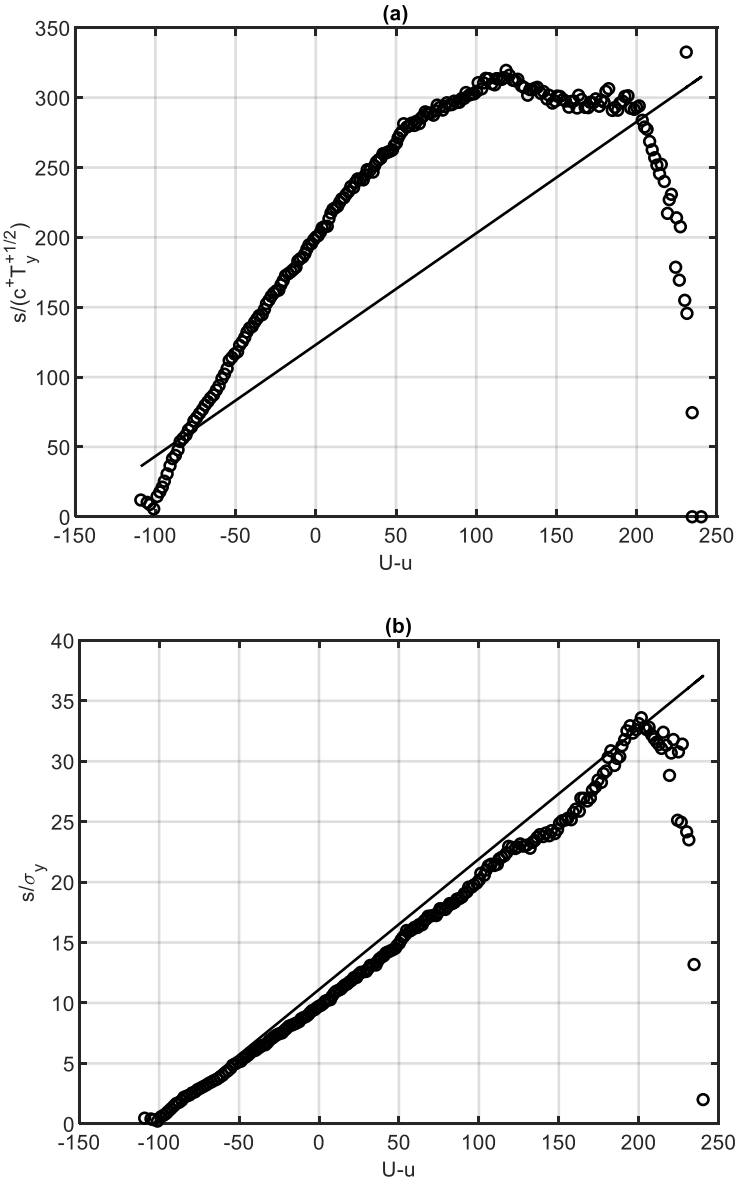

Fig. B6. Ratio of (a) particle shear stress *s* and the product of particle concentration of ascending particles and the square root of T_y^+ and (b) particle shear stress and the particle normal stress as functions of the velocity difference, *U*-*u*, measured in numerical simulations of saltation in a viscous shearing flow with d_w = 1, St = 100, *r* = 150000, Sh = 0.05 (so that the Stokes drag is dominant and C_D = 18/St = 0.18) and *M* = 0.0004. The solid lines are the predictions of equations (B19) and (B20), respectively.

B2. Saltation in turbulent shearing flows

In the limit of large $C_D\xi_y^+$, using equations (A17), (A20) and (B2) into equation (B14), and integrating, we obtain the following expression, in the case of saltation in turbulent shearing flows,

$$s = -\frac{c^+}{\pi\sqrt{T_x^+ T_y^+}}\int_0^{+\infty}\xi_y^+\exp\left(-\frac{\xi_y^{+2}}{2T_y^+}\right)\int_{-\infty}^{+\infty}\left\{\left(\xi_x^+ - u\right) + u - U - 0.85\frac{\sqrt{rS}}{\kappa}\left[\ln\left(\frac{\kappa\xi_y^+}{C_D\sqrt{rS}}\frac{\mathrm{d}U}{\mathrm{d}y}+1\right)\right]\right\}$$
$$\times\exp\left[-\frac{\left(\xi_x^+ - u\right)^2}{2T_x^+}\right]\mathrm{d}\xi_x^+\mathrm{d}\xi_y^+$$
$$= \frac{c^+}{\pi\sqrt{T_x^+ T_y^+}}\sqrt{\pi 2T_x^+}\int_0^{+\infty}\xi_y^+\left\{U + 0.85\frac{\sqrt{rS}}{\kappa}\left[\ln\left(\frac{\kappa\xi_y^+}{C_D\sqrt{rS}}\frac{\mathrm{d}U}{\mathrm{d}y}+1\right)\right] - u\right\}\exp\left(-\frac{\xi_y^{+2}}{2T_y^+}\right)\mathrm{d}\xi_y^+$$
$$\simeq c^+\sqrt{\frac{2T_y^+}{\pi}}\left[U - u + 0.85\frac{\sqrt{rS}}{\kappa}\ln\left(\frac{\kappa}{C_D}\sqrt{\frac{T_y^+}{rS}}\frac{\mathrm{d}U}{\mathrm{d}y}+1\right)\right] \simeq \frac{3}{5}C_D\sigma_y\left[U - u + \frac{3}{4}\frac{\sqrt{rS}}{\kappa}\ln\left(\frac{\kappa}{C_D}\sqrt{\frac{T_y^+}{rS}}\frac{\mathrm{d}U}{\mathrm{d}y}+1\right)\right], \quad \text{(B21)}$$

where we have taken $\xi_y^+ \approx \sqrt{T_y^+}$ in the argument of the logarithm to carry out the analytical integration, and, we have kept the same dependency on the drag coefficient and the normal stress as in the case of saltation in viscous shearing flows (equation B20). The factor 3/4 in front of the logarithm allows to better fit the results of discrete-continuum simulations of saltation in turbulent shearing flows.

Appendix C. Boundary conditions for shallow impacts at a rigid, bumpy bed

After Lämmel et al. (2017), in the case of angle of impact θ much less than $\pi/2$ (shallow impact) of particles with large coefficient of friction, the negative of the average ratio of the vertical particle velocity after and before the impact is

$$\left\langle -\frac{\xi_{y,0}^{+}}{\xi_{y,0}^{-}} \right\rangle = -e_t + \frac{2}{3}\left(e_n + e_t\right)\sqrt{\frac{2}{\theta}\frac{2d_w}{1+d_w}}, \tag{C1}$$

where e_n and e_t are the coefficients of normal and tangential restitution, respectively, and, here and in what follows, we use the subscript 0 to indicate quantities evaluated at the bed.

In the limit of large take-off velocity, equations (A8), (A12) and (24) give

$$\theta = \tan\left(-\xi_{y,0}^{-}/\xi_{x,0}^{-}\right) \simeq \frac{C_D}{\mathrm{St}\left(\mathrm{Sh}-s_0\right)}, \tag{C2}$$

for saltation in viscous shearing flows.

In the case of saltation in turbulent shearing flows, instead, in the limit of large take-off velocity, equations (A8), (A17) and (A20) give

$$\theta \simeq \left[0.85 C_D \frac{\sqrt{r\left(\mathrm{Sh}-s_0\right)}}{\kappa} \ln\left(\frac{1}{C_D}\frac{\sqrt{T_{y,0}^{+}}}{y_0}\right)\right]^{-1}, \tag{C3}$$

with $\xi_{y,0}{}^{+} \simeq \sqrt{T_{y,0}^{+}}$.

By inserting equation (A8) into equation (C1), we obtain

$$\left\langle \xi_{y,0}^{+} \right\rangle = -\frac{e_t}{C_D} + \frac{2\sqrt{2}}{3}\left(e_n + e_t\right)\frac{1}{C_D\theta^{1/2}}\sqrt{\frac{2d_w}{1+d_w}}. \tag{C4}$$

Then, we can assume that $T_{y,0}^{+} = \left\langle \left(\xi_{y,0}^{+}\right)^2 \right\rangle \propto \left\langle \xi_{y,0}^{+} \right\rangle^2$, so that at leading order,

$$T_{y,0}^{+} = \alpha_T \frac{1}{C_D{}^2\theta}\frac{2d_w}{1+d_w}, \tag{C5}$$

with the coefficient of proportionality α_T weakly dependent on the coefficients of normal and tangential restitution and, perhaps, on the flow regime of the fluid. Lämmel et al. (2017) also obtained

$$\left\langle \frac{\left(\xi_{y,0}^{+}\right)^2 + \left(\xi_{x,0}^{+}\right)^2}{\left(\xi_{y,0}^{-}\right)^2 + \left(\xi_{x,0}^{-}\right)^2} \right\rangle = \left[e_t - \frac{\left(e_t{}^2 - e_n{}^2\right)}{2e_t}\theta\frac{2d_w}{1+d_w}\right]^2, \tag{C6}$$

so that, with equations (A8) and (A12), and $\left\langle \left(\xi_{x,0}^{+}\right)^2 \right\rangle \propto \left\langle \xi_{x,0}^{+} \right\rangle^2 = \left(u_0^{+}\right)^2$,

$$u_0^{+} \propto \sqrt{\frac{1}{C_D{}^2}\left(1+\frac{1}{\theta^2}\right)\left[e_t - \frac{\left(e_t{}^2 - e_n{}^2\right)}{2e_t}\theta\frac{2d_w}{1+d_w}\right]^2 - T_{y,0}^{+}}. \tag{C7}$$

Then, we can determine the total particle slip velocity at the bed as

$$u_0 = \frac{c_0^{+} u_0^{+} + c_0^{-} u_0^{-}}{c_0}. \tag{C8}$$

With equations (B5) and (B6), and u_0^{-} given by equation (A12), we obtain, at leading order,

$$u_0 = \alpha_u \frac{1}{C_D \theta}, \tag{C9}$$

where, once again, the coefficient of proportionality α_u is a weak function of the coefficients of restitution and the flow regime of the fluid. Using equation (C5) into equation (C9) gives

$$u_0 = \frac{\alpha_u}{\alpha_T} \frac{1 + d_w}{2 d_w} C_D T_{y,0}^{+}. \tag{C10}$$

Appendix D. Discrete-continuum numerical simulations

The discrete-continuum (DC) simulations is based on the combination of a discrete element method for the particle dynamics coupled to a continuum description of hydrodynamics, as developed in Durán et al. (2012), Ralaiarisoa *et al.* (2020) and Valance et al. (2022).

The particle motion is described by a Lagrangian approach according to which the particle labelled *p* obeys the following dimensionless equations:

$$\frac{\mathrm{d}\boldsymbol{\xi}^p}{\mathrm{d}t} = -\mathbf{e}_y + \sum_q \mathbf{f}_c^{p,q} + \mathbf{f}_{drag}^p \tag{D1}$$

$$I\frac{\mathrm{d}\boldsymbol{\omega}^p}{\mathrm{d}t} = \frac{1}{2}\sum_q \mathbf{n}^{p,q} \times \mathbf{f}_c^{p,q} \tag{D2}$$

where $\boldsymbol{\xi}^p$ and $\boldsymbol{\omega}^p$ are the translational and angular velocity vectors of particle *p,* respectively; $\mathbf{e}_x$ and $\mathbf{e}_y$ are the horizontal and vertical unit vectors, respectively; $\mathbf{f}_{drag}^p = C_D\left[\left(U-\xi_x^p\right)\mathbf{e}_x - \xi_y^p\mathbf{e}_y\right]$ is the dimensionless drag force exerted by the fluid on the *p*-particle and $\mathbf{f}_c^{p,q}$ is the dimensionless contact force between particles *p* and *q*; $I = 1/10$ is the moment of inertia of a sphere; and $\mathbf{n}^{p,q}$ is the unit vector along the contact direction.

The normal component $f_{c,n}$ of the contact force is modelled by a linear spring dashpot, so that $f_{c,n} = (k_n\delta + \gamma_n v_n)$, where k_n is the spring stiffness, δ the overlap between the compliant spheres, γ_n the viscous damping coefficient and v_n the normal component of the relative translational particle velocities. The negative of the ratio between the normal relative velocity before and after the collision is the coefficient of normal restitution e_n. If the values of e_n and k_n are prescribed, γ_n is deduced from the following relation: $\gamma_n = (\pi/6)\sqrt{12k_n/(1+\pi^2/\ln(e_n)^2)}$. The tangential component $f_{c,t}$ of the contact force is described via a Coulomb friction model regularized through a viscous damping: $f_{c,t} = -\min(\mu f_{c,n}, \gamma_t v_t)\mathrm{sign}(v_t)$, where μ is the Coulomb friction coefficient, v_t the relative slip velocity at contact and γ_t the tangential viscous damping coefficient. The values chosen for the parameters are: $k_n = \mathrm{p}/6\cdot 10^7$, $\gamma_n = \gamma_t$, $e_n = 0.88$, and $\mu = 0.5$.

The fluid motion is solved by an Eulerian description based on Eq. (24) or Eq. (37) for laminar and turbulent flows, respectively. The vertical component of the fluid velocity is assumed to be zero, so that only the horizontal momentum balance is required and reads

$$\frac{\mathrm{d}S}{\mathrm{d}y} = F_x, \tag{D3}$$

where $F_x = c < \sum_{p\epsilon[y;\, y+dy]} C_D(U-\xi_x) > / < \sum_{p\epsilon[y;\, y+dy]} 1 >$, with the angular brackets denoting ensemble averaging, represents the *x*-component of the average volume force exerted on the fluid by the particles whose centers are located in the horizontal slice between *y* and *y*+d*y*. The integration of equation (D3) gives

$$S = \mathrm{Sh} - \int_0^\infty F_x \mathrm{d}y, \tag{D4}$$

where the infinite upper bound of the integral means that all moving grains located above *y* must be accounted for. Once the vertical profile *S*(*y*) of the fluid shear stress is determined, the horizontal fluid velocity profile can then be obtained from the integration Eq. (24) or Eq. (37) for laminar and turbulent shearing flows, respectively, with the no-slip boundary condition $U = 0$ at $y = 0$.

The simulated system is quasi-two-dimensional with a streamwise length equal to 5120 particle diameters and a transverse length equal to one diameter. We use spherical particles with a polydispersity of ±10 % and adjust their number in the system to obtain the desired value of the mass hold-up M. Periodic boundary conditions are employed in the streamwise direction. The domain is not upper bounded, while the lower boundary is composed of a layer of immobile particles of diameter d_w in close contact (rigid, bumpy bed; see Figure 1). As mentioned earlier in the paper, we suppress the possibility of particle–particle collisions above the bed.

Operatively, at every time step, we integrate equations (D1) and (D2) for every particle in the system and determine its new velocity and position. We then use this information to update the profiles of fluid shear stress and horizontal velocity via equations (4), and (24) for viscous flows or equation (37) for turbulent flows and proceed with the next time step until we reach a steady state, that is, when the horizontal mass flux averaged over a window of 100 unit time steps is stationary. Initially, the fluid profile is taken to be linear or logarithmic for viscous and turbulent shearing flows, respectively, and corresponds to the unperturbed profile in the absence of particles. The particles are initially displayed on a horizontal row located at ten diameters from the rigid, bumpy bed, with a constant inter-particle distance equal to two diamters and zero initial velocity. Importantly, the final state is independent of the initial conditions as long as the number of particles in the flow does not surpass its transport capacity.